14. Spatial Pattern Formation with Reaction/Population Interaction Diffusion Mechanisms

14.1 Role of Pattern in Developmental Biology

Embryology is that part of biology which is concerned with the formation and development of the embryo from fertilization until birth. Development of the embryo is a sequential process and follows a ground plan, which is usually laid down very early in gestation. In humans for example it is set up roughly by the 5th week. The book by Slack (1983) is a readable account of the early stages of development from egg to embryo.

Morphogenesis, the part of embryology with which we shall be concerned, is the development of pattern and form. How the developmental ground plan is established is unknown as are the mechanisms which produce the spatial patterning necessary for specifying the various organs. The following three chapters and most of this one will be devoted to mechanisms which can generate spatial pattern and form, and which have been proposed as possible pattern formation processes in a variety of morphogenetic situations. Section 14.7 will be concerned with an important ecological aspect of pattern formation, which suggests possible strategies of pest control – the mathematical analysis is different but highly relevant to many embryological situations.

Cell division starts after fertilisation. When sufficient cell division has taken place in a developing embryo the key problem is how the homogeneous mass of cells are spatially organised so that the sequential process of development can progress. Cells differentiate, in a biological sense, according to where they are in the spatial organisation. They also move around in the embryo. This latter phenomenon is an important element in morphogenesis and has given rise to a new approach to the generation of pattern and form discussed in some detail in Chapter 17.

It is impossible not to be fascinated and enthralled with the wealth, diversity and beauty of pattern in biology. Fig. 14.1 shows only four examples. How such patterns, and millions of others, were laid down is still unknown. The patterning problems posed by only Fig. 14.1 are quite diverse.

As a footnote to Fig. 14.1 (c), note the antennae on the moth. These antennae very effectively collect molecules of the chemical odorant, called a pheromone, which is exuded by the female to attract the male. The filtering efficiency of such antennae, which collect, and in effect count, the molecules, poses a very different

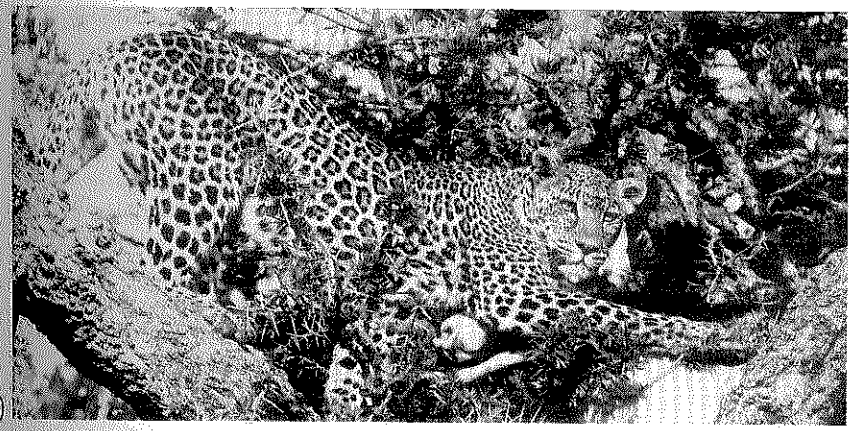

(a)

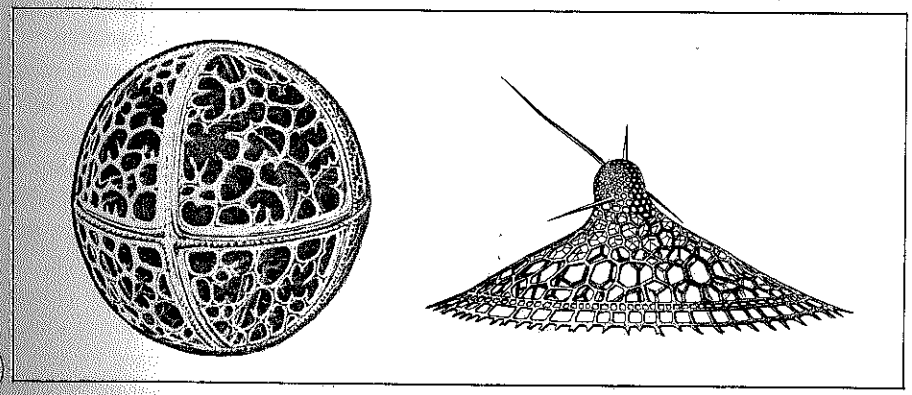

(b)

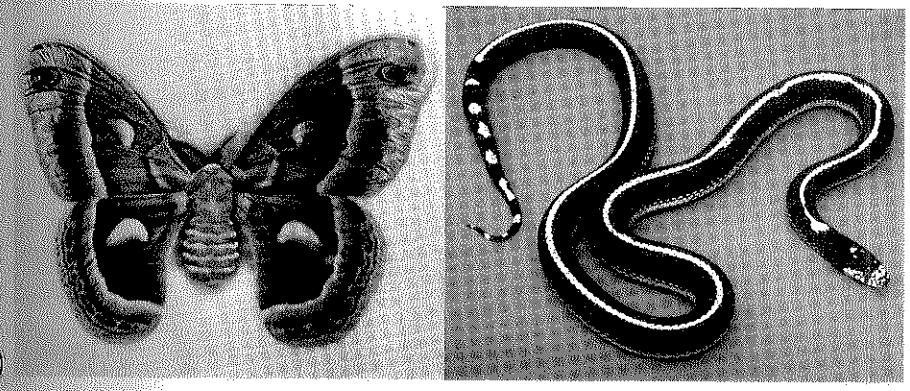

(c) (d)

Fig. 14.1a-d. (a) Leopard (*Panthera pardus*) in the Serengetti National Park, Tanzania. Note the individual spot structure. (Photograph courtesy of Hans Kruuk) (b) Radiolarians (*Trissocyclus spaeridium* and *Eucecryphalus genbouri*). These are small marine organisms – protozoa – of the order of a millimeter across. (After Haeckel 1862, 1887) The structural architecture of radiolarians is amazingly diverse (see, for example, the plate reproductions of some of Haeckel's drawings in the Dover Archive Series, Haeckel 1974). (c) Moth (*Hyalophora cecropia*). As well as the wing patterns note the stripe pattern on the body and the structure of the antennae. (d) Californian king snake. Sometimes the pattern consists of crossbands rather than a backstripe. (Photograph courtesy of Lloyd Lemke)

and interesting mathematical biology problem to those discussed in this book, namely how such a filter antenna should be designed to be most efficient. This specific problem is discussed in detail by Murray (1977).

The fundamental importance of pattern and form in developmental biology is self-evident. Whatever pattern we observe in the animal world it is almost certain that the process that produced it is unknown. Although the mechanism must be genetically controlled, the genes themselves cannot create the pattern. They only provide a blue-print or recipe, for the pattern generation. One of the major problems in biology is how genetic information is physically translated into the necessary pattern and form. Much of the research in developmental biology, both experimental and theoretical, is devoted to trying to determine the underlying mechanisms which generate pattern and form in early development. The detailed discussion in these next few chapters discusses some of the mechanisms which have been proposed and gives an indication of the role of mathematical modelling in trying to unravel the underlying mechanisms involved in morphogenesis.

A phenomenological concept of pattern formation and differentiation called *positional information* was proposed by Wolpert (1969, see the reviews in 1971, 1981). He suggested that cells are pre-programmed to react to a chemical (or morphogen) concentration and differentiate accordingly, into different kinds of cells such as cartilage cells. The general introductory paper by Wolpert (1977) gives a very clear and non-technical description of development of pattern and form in animals and the concepts and application of positional information.

The chemical prepattern viewpoint of embryogenesis separates the process of development into several steps; the essential first step is the creation of a morphogen concentration spatial pattern. The name 'morphogen' is used for such a chemical because it effects morphogenesis. The notion of positional information relies on a chemical pre-specification so that the cell can read out its position in the coordinates of chemical concentration, and differentiate, undergo appropriate cell shape change, or migrate accordingly. So, once the prepattern is established, morphogenesis is a slave process. Positional information is not dependent on the specific mechanism which sets up the spatial prepattern of morphogen concentration. This chapter is concerned with reaction diffusion models as the possible mechanisms for generating biological pattern. The basic chemical theory or reaction diffusion theory of morphogenesis was put forward in the classical paper by Turing (1952). Levin and Segel (1985) give a brief and readable survey of reaction diffusion theories and their generalisations.

With the complexity of animal forms the concept of positional information necessarily implies a very sophisticated interpretation of the 'morphogen map' by the cell. This need not pose any problem when we recall how immensely complex a cell is. A rough idea, for example, is given by comparing the weight per bit of information of the cell's DNA molecule, around 10^{-22}, to that of, say, imaging by an electron beam of around 10^{-10} or of a magnetic tape of about 10^{-5}. The most sophisticated and compact computer chip is simply not in the same class as a cell.

14.2 Reaction Diffusion (Turing) Mechanisms

Turing (1952) suggested that, under certain conditions, chemicals can react and diffuse in such a way as to produce steady state heterogeneous spatial patterns of chemical or morphogen concentration. In Section 9.2 in Chapter 9 we derived the governing equations for reaction diffusion mechanisms, namely (9.16), which we consider here in the form:

$$\frac{\partial \mathbf{c}}{\partial t} = \mathbf{f}(\mathbf{c}) + D\nabla^2 \mathbf{c}\,, \tag{14.1}$$

where $\mathbf{c}$ is the vector of morphogen concentrations, $\mathbf{f}$ represents the reaction kinetics and D is the diagonal matrix of positive constant diffusion coefficients. This chapter will mainly be concerned with models for two chemical species, $A(\mathbf{r},t)$ and $B(\mathbf{r},t)$ say. The equation system is then of the form

$$\begin{aligned} \frac{\partial A}{\partial t} &= F(A,B) + D_A\nabla^2 A\,, \\ \frac{\partial B}{\partial t} &= G(A,B) + D_B\nabla^2 B\,, \end{aligned} \tag{14.2}$$

where F and G are the kinetics, which will always be nonlinear.

Turing's (1952) idea is a simple but profound one. He said that if, in the absence of diffusion (effectively $D_A = D_B = 0$), A and B tend to a linearly stable uniform steady state then, under certain conditions, which we shall derive, spatially inhomogeneous patterns can evolve by *diffusion driven instability* if $D_A \neq D_B$. Diffusion is usually considered a *stabilising* process which is why this was such a novel concept. To see intuitively how diffusion can be destabilising consider the following, albeit unrealistic, but informative analogy.

Consider a field of dry grass in which there is a large number of grasshoppers which can generate a lot of moisture by sweating if they get warm. Now suppose the grass is set alight at some point and a flame front starts to propagate. We can think of the grasshopper as an inhibitor and the fire as an activator. If there was no moisture to quench the flames the fire would simply spread over the whole field which would result in a uniform charred area. Suppose, however, that when the grasshoppers get warm enough they can generate enough moisture to dampen the grass so that when the flames reach such a pre-moistened area the grass will not burn. The scenario for spatial pattern is then as follows. The fire starts to spread – it is one of the 'reactants', the activator, with a 'diffusion' coefficient D_F say. When the grasshoppers, the inhibitor 'reactant', ahead of the flame front feel it coming they move quickly well ahead of it – that is they have a 'diffusion' coefficient, D_G say, which is much larger that D_F. The grasshoppers then sweat profusely and generate enough moisture and thus prevent the fire spreading into the moistened area. In this way the charred area is restricted to a finite domain which depends on the 'diffusion' coefficients of the reactants – fire and grasshoppers – and various 'reaction' parameters. If, instead of a single initial

fire, there was a random scattering of them we can see how this process would result in a final spatially inhomogeneous steady state distribution of charred and uncharred regions in the field, since around each fire the above scenario would take place. It is clear that if the grasshoppers and flame front 'diffused' at the same speed no such spatial pattern could evolve. It is clear how to construct other analogies: another example is given in the Scientific American article by Murray (1988).

In the following section we shall describe the process in terms of reacting and diffusing morphogens and derive the necessary conditions on the reaction kinetics and diffusion coefficients. We shall also derive the type of spatial patterns we might expect. Here we briefly record for subsequent use two particularly simple hypothetical systems and one experimentally realised example, which are capable of satisfying Turing's conditions for a pattern formation system. There are now, of course, many other systems which have been used in studies of spatial patterning. These have varying degrees of experimental plausibility. With the extensive discussion of the Belousov-Zhabotinskii reaction in Chapters 7 and 12 we should particularly note it as perhaps the major experimental system.

The simplest system is the Schnakenberg (1979) reaction discussed in Chapter 6 which, with reference to the system form (14.2), has kinetics

$$F(A,B) = k_1 - k_2A + k_3A^2B, \quad G(A,B) = k_4 - k_3A^2B\ , \tag{14.3}$$

where the k's are the positive rate constants. Here A is created autocatalytically by the k_3A^2B term in $F(A,B)$. This is one of the prototype reaction diffusion systems. The second is the activator-inhibitor mechanism suggested by Gierer and Meinhardt (1972) and discussed in Chapter 5, namely

$$F(A,B) = k_1 - k_2A + \frac{k_3A^2}{B}, \quad G(A,B) = k_4A^2 - k_5B\ , \tag{14.4}$$

where here A is the activator and B the inhibitor. The k_3A^2/B term is again autocatalytic. The third, the real empirical substrate-inhibition system studied experimentally by Thomas (1975) and also described in detail in Chapter 5, has

$$\begin{aligned} &F(A,B) = k_1 - k_2A - H(A,B), \quad G(A,B) = k_3 - k_4B - H(A,B)\ , \\ &H(A,B) = \frac{k_5AB}{k_6 + k_7A + k_8A^2}\ . \end{aligned} \tag{14.5}$$

Here A and B are respectively the concentrations of the substrate oxygen and the enzyme uricase. The substrate inhibition is evident in the H-term via k_8A^2. Since the H-terms are negative they contribute to reducing A and B; the rate of reduction is inhibited for large enough A.

Before commenting on the types of reaction kinetics capable of generating pattern we must nondimensionalise the systems given by (14.2) with reaction kinetics from (14.3)–(14.5). By way of example we carry out the details here for

(14.2) with F and G given by (14.3). Introduce L as a typical length scale and set

$$\begin{aligned} &u = A\left(\frac{k_3}{k_2}\right)^{1/2}, \quad v = B\left(\frac{k_3}{k_2}\right)^{1/2}, \quad t^* = \frac{D_At}{L^2}, \quad \mathbf{x}^* = \frac{\mathbf{x}}{L}\ , \\ &d = \frac{D_B}{D_A}, \quad a = \frac{k_1}{k_2}\left(\frac{k_3}{k_2}\right)^{1/2}, \\ &b = \frac{k_4}{k_2}\left(\frac{k_3}{k_2}\right)^{1/2}, \quad \gamma = \frac{L^2k_2}{D_A}\ . \end{aligned} \tag{14.6}$$

The dimensionless reaction diffusion system becomes, on dropping the asterisks for algebraic convenience,

$$\begin{aligned} u_t &= \gamma(a - u + u^2v) + \nabla^2u = \gamma f(u,v) + \nabla^2u\ , \\ v_t &= \gamma(b - u^2v) + d\nabla^2v = \gamma g(u,v) + d\nabla^2v\ , \end{aligned} \tag{14.7}$$

where f and g are defined by these equations. We could incorporate γ into new length and time scales by setting $\gamma^{1/2}\mathbf{r}$ and γt for $\mathbf{r}$ and t respectively. This is equivalent to defining the length scale L such that $\gamma = 1$, that is $L = (D_A/k_2)^{1/2}$. We retain the specific form (14.7) for reasons which will become clear shortly as well as for the analysis in the next section and for the applications in Chapter 15.

An appropriate nondimensionalisation of the reaction kinetics (14.4) and (14.5) give (see Exercise 1)

$$\begin{aligned} &f(u,v) = a - bu + \frac{u^2}{v}, \quad g(u,v) = u^2 - v\ , \\ &f(u,v) = a - u - h(u,v), \quad g(u,v) = \alpha(b - v) - h(u,v)\ , \\ &h(u,v) = \frac{\rho uv}{1 + u + Ku^2}\ , \end{aligned} \tag{14.8}$$

where a, b, α, ρ and K are positive parameters. If we include activator inhibition in the activator-inhibitor system in the first of these we have, for f and g,

$$f(u,v) = a - bu + \frac{u^2}{v(1 + ku^2)}, \quad g(u,v) = u^2 - v\ , \tag{14.9}$$

where k is a measure of the inhibition: see also Section 5.5 in Chapter 5. Murray (1982) discussed each of these systems in detail and drew conclusions as to their relative merits as pattern generators. For most pattern formation illustrations the simplest, namely (14.7), turns out to be the most robust and of course the easiest to study.

All such reaction diffusion systems can be nondimensionalised and scaled to take the general form

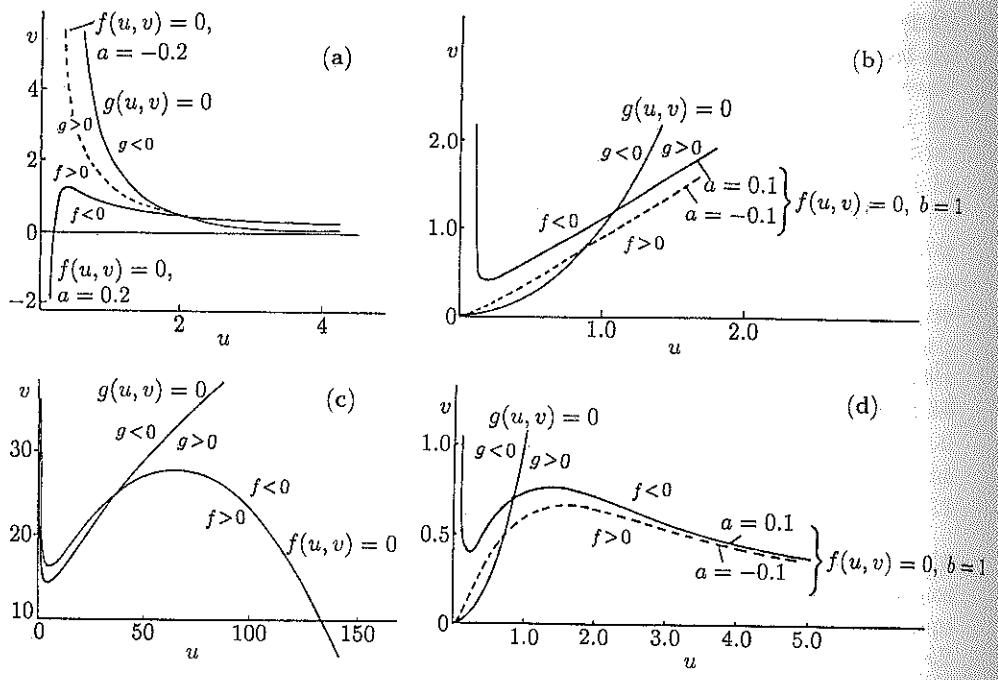

Fig. 14.2a-d. Null clines $f(u,v)=0$, $g(u,v)=0$: (a) The dimensionless Schnakenberg (1979) kinetics (14.7) with $a=0.2$ and $b=2.0$ with the dashed curve, where $a=-0.2$ and which is typical of the situation when $a<0$. (b) The dimensionless Gierer and Meinhardt (1972) system with $a=\pm 0.1$, $b=1$ and no activator inhibition. (c) The empirical Thomas (1975) system defined by (14.8) with parameter values $a=150$, $b=100$, $\alpha=1.5$, $\rho=13$, $K=0.05$. (d) The kinetics in (14.9) with $a>0$, $b>0$ and $k>0$, which implies activator inhibition – the dashed curve has $a<0$.

where d is the ratio of diffusion coefficients and γ can have any of the following interpretations:

(i) $\gamma^{1/2}$ is proportional to the *linear* size of the spatial domain in one dimension. In two dimensions γ is proportional to the area. This meaning is particularly important as we shall see later in Section 14.5 and in Chapter 15.

(ii) γ represents the relative strength of the reaction terms. This means, for example, that an increase in γ may represent an increase in activity of some rate-limiting step in the reaction sequence.

(iii) An increase in γ can also be thought of as equivalent to a decrease in the diffusion coefficient ratio d.

Particular advantages of this general form are: (a) the dimensionless parameters γ and d admit a wider biological interpretation than do the dimensional parameters and (b) when we consider the domains in parameter space where particular spatial patterns appear, the results can be conveniently displayed in (γ, d) space. This aspect was exploited by Arcuri and Murray (1986).

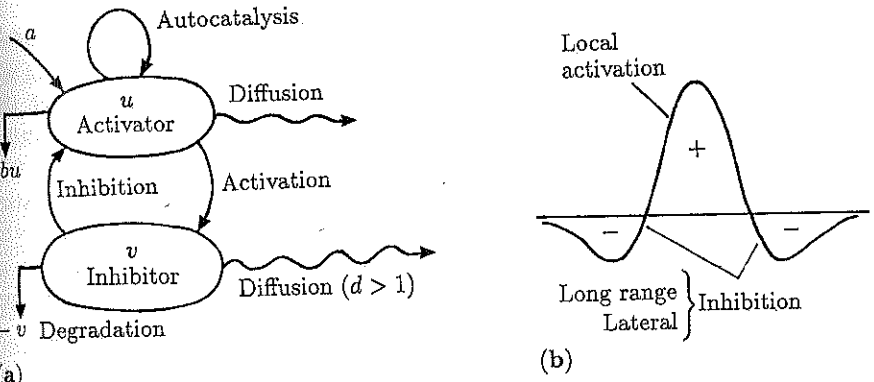

Fig. 14.3a,b. (a) Schematic representation of the activator-inhibitor system

$$u_t = a - bu + \frac{u^2}{v} + \nabla^2 u, \quad v_t = u^2 - v + d\nabla^2 v\,.$$

(b) Spatial representation of local activation and long range inhibition.

Whether or not the systems (14.2) are capable of generating Turing-type spatial patterns crucially depends on the reaction kinetics f and g, and the values of γ and d. The detailed form of the null clines provides essential initial information. Fig. 14.2 illustrates typical null clines for f and g defined by (14.7)–(14.9).

In spite of their different chemical motivation and derivation all of these kinetics are equivalent to some activation-inhibition interpretation and when coupled with unequal diffusion of the reactants, are capable of generating spatial patterns. The spatial activation-inhibition concept was discussed in detail in Section 9.5 in Chapter 9, and arose from an integral equation formulation: refer to equation (9.41). As we shall see in the next section the crucial aspect of the kinetics regarding pattern generation is incorporated in the form of the null clines and how they intersect in the vicinity of the steady state. There are two broad types illustrated in the last figure. The steady state neighbourhood of the null clines in Fig. 14.2 (b), (c), (d) are similar and represent one class, while that in Fig. 14.2 (a) is the other.

We should note here that there are other important classes of null clines which we do not consider, such as those in which there is more than one positive steady state: we discussed such kinetics in Chapter 6 for example. Reaction diffusion systems with such kinetics can generate even more complex spatial patterns: initial conditions here are particularly important. We also do not discuss here systems in which the diffusion coefficients are space dependent and concentration, or population, dependent: these are more important in ecological contexts. We briefly considered density dependent diffusion cases in Chapter 9.

It is often useful and intuitively helpful in model building to express the mechanism's kinetics in schematic terms with some convention to indicate autocatalysis, activation, inhibition, degradation and unequal diffusion. If we do this,

by way of illustration, with the activator-inhibitor kinetics given by the first of (14.8) in (14.10) we can adopt the convention shown in Fig. 14.3 (a).

The effect of different diffusion coefficients, here with $d > 1$, is to give the prototype spatial concept of local activation and lateral inhibition illustrated in Fig. 14.3 (b). The general concept was introduced before in Section 9.5: see Fig. 9.5. It is this generic spatial behaviour which is necessary for spatial patterning – the grasshoppers and the fire analogy is an obvious example with the fire the local activation and the grasshoppers providing the long range inhibition. It is intuitively clear that the diffusion coefficient of the inhibitor must be larger than that of the activator.

14.3 Linear Stability Analysis and Evolution of Spatial Pattern: General Conditions for Diffusion-Driven Instability

A reaction diffusion system exhibits diffusion-driven instability or *Turing instability* if the homogeneous steady state is stable to small perturbations in the absence of diffusion but unstable to small *spatial* perturbations when diffusion is present. The usual concept of instability in biology is in the context of ecology, where a uniform steady state becomes unstable to small perturbations and the populations typically exhibit some temporal oscillatory behaviour. The instability we are concerned with here is of a quite different kind. The mechanism driving the spatially inhomogeneous instability is diffusion: the mechanism determines the spatial pattern that evolves. How the pattern or mode is selected is an important aspect of the analysis.

We derive here the necessary and sufficient conditions for diffusion driven instability of the steady state and the initiation of spatial pattern for the general system (14.10). To formulate the problem mathematically we require boundary and initial conditions. These we take to be zero flux boundary conditions and given initial conditions. The mathematical problem is then defined by

$$\begin{aligned} &u_t = \gamma f(u,v) + \nabla^2 u, \quad v_t = \gamma g(u,v) + d\nabla^2 v\,, \\ &(\mathbf{n}\cdot\nabla)\begin{pmatrix} u \\ v \end{pmatrix} = 0, \quad \mathbf{r} \text{ on } \partial B; \quad u(\mathbf{r},0),\ v(\mathbf{r},0) \text{ given}\,, \end{aligned} \tag{14.11}$$

where ∂B is the closed boundary of the reaction diffusion domain B and $\mathbf{n}$ is the unit outward normal to ∂B. There are several reasons for choosing zero flux boundary conditions. The major one is that we are interested in self-organisation of pattern; zero flux conditions imply no external input. If we imposed fixed boundary conditions on u and v the spatial patterning could be a direct consequence of the boundary conditions as we shall see in the ecological problem below in Section 14.7. Another biologically reasonable set of conditions is periodicity: these correspond to closed three-dimensional boundaries. In Section 14.4

we carry out the analysis for a specific one- and two-dimensional situation with the kinetics given by (14.7).

The relevant homogeneous steady state (u_0, v_0) of (14.11) is the positive solution of

$$f(u,v) = 0, \quad g(u,v) = 0\,. \tag{14.12}$$

Since we are concerned with *diffusion driven* instability we are interested in linear instability of this steady state that is solely *spatially* dependent. So, in the absence of any spatial variation the homogeneous steady state must be linearly stable: we first determine the conditions for this to hold. These were derived in Chapter 3 but as a reminder and for notational completeness we briefly rederive them here.

With no spatial variation u and v satisfy

$$u_t = \gamma f(u,v), \quad v_t = \gamma g(u,v)\,. \tag{14.13}$$

Linearising about the steady state (u_0, v_0) in exactly the same way as we did in Chapter 3, we set

$$\mathbf{w} = \begin{pmatrix} u - u_0 \\ v - v_0 \end{pmatrix} \tag{14.14}$$

and (14.13) becomes, for $|\mathbf{w}|$ small,

$$\mathbf{w}_t = \gamma A\mathbf{w}, \quad A = \begin{pmatrix} f_u & f_v \\ g_u & g_v \end{pmatrix}_{u_0,v_0}, \tag{14.15}$$

where A is the stability, or community, matrix. From now on we shall take the partial derivatives of f and g to be evaluated at the steady state unless stated otherwise. We now look for solutions in the form

$$\mathbf{w} \propto e^{\lambda t} \tag{14.16}$$

where λ is the eigenvalue. The steady state $\mathbf{w} = 0$ is linearly stable if $\mathrm{Re}\,\lambda < 0$ since in this case the perturbation $\mathbf{w} \to 0$ as $t \to \infty$. Substitution of (14.16) into (14.15) determines the eigenvalues λ as the solutions of

$$\begin{aligned} |\gamma A - \lambda I| &= \begin{vmatrix} \gamma f_u - \lambda & \gamma f_v \\ \gamma g_u & \gamma g_v - \lambda \end{vmatrix} = 0 \\ \Rightarrow \quad &\lambda^2 - \gamma(f_u + g_v)\lambda + \gamma^2(f_u g_v - f_v g_u) = 0\,, \end{aligned} \tag{14.17}$$

so

$$\lambda_1, \lambda_2 = \frac{1}{2}\gamma\left[(f_u + g_v) \pm \{(f_u + g_v)^2 - 4(f_u g_v - f_v g_u)\}^{1/2}\right]\,. \tag{14.18}$$

Linear stability, that is $\mathrm{Re}\,\lambda < 0$, is guaranteed if

$$\mathrm{tr}\,A = f_u + g_v < 0, \quad |A| = f_u g_v - f_v g_u > 0\,. \tag{14.19}$$

Since (u_0, v_0) are functions of the parameters of the kinetics, these inequalities thus impose certain constraints on the parameters. Note that for all cases in Fig. 14.2 in the neighbourhood of the steady state, $f_u > 0$, $g_v < 0$, and for Fig. 14.2 (a) $f_v > 0$, $g_u < 0$ while for Fig. 14.2 (b)–(d) $f_v < 0$, $g_u > 0$. So $\mathrm{tr}\, A$ and $|A|$ could be positive or negative: here we are only concerned with the conditions and parameter ranges which satisfy (14.19).

Now consider the full reaction diffusion system (14.11) and again linearise about the steady state, which with (14.14) is $\mathbf{w} = 0$, to get

$$\mathbf{w}_t = \gamma A\mathbf{w} + D\nabla^2\mathbf{w}, \quad D = \begin{pmatrix} 1 & 0 \\ 0 & d \end{pmatrix} . \tag{14.20}$$

To solve this system of equations subject to the boundary conditions (14.11) we first define $\mathbf{W}(\mathbf{r})$ to be the time independent solution of the spatial eigenvalue problem defined by

$$\nabla^2\mathbf{W} + k^2\mathbf{W} = 0, \quad (\mathbf{n}\cdot\nabla)\mathbf{W} = 0 \quad \text{for} \quad \mathbf{r} \text{ on } \partial B , \tag{14.21}$$

where k is the eigenvalue. For example, if the domain is one-dimensional, say $0 \le x \le a$, $\mathbf{W} \propto \cos(n\pi x/a)$ where n is an integer: this satisfies zero flux conditions at $x = 0$ and $x = a$. The eigenvalue in this case is $k = n\pi/a$. So $1/k = a/n\pi$ is a measure of the wave-like pattern: the eigenvalue k is called the *wavenumber* and $1/k$ is proportional to the wavelength ω_c; $\omega_c = 2\pi/k = 2a/n$ in this example. From now on we shall refer to k in this context as the wavenumber. With finite domains there is a discrete set of possible wavenumbers.

Let $\mathbf{W}_k(\mathbf{r})$ be the eigenfunction corresponding to the wavenumber k. Each eigenfunction $\mathbf{W}_k$ satisfies zero flux boundary conditions. Because the problem is linear we now look for solutions $\mathbf{w}(\mathbf{r}, t)$ of (14.20) in the form

$$\mathbf{w}(\mathbf{r}, t) = \sum_k c_k e^{\lambda t}\mathbf{W}_k(\mathbf{r}) . \tag{14.22}$$

where the constants c_k are determined by a Fourier expansion of the initial conditions in terms of $\mathbf{W}_k(\mathbf{r})$. λ is the eigenvalue which determines temporal growth. Substituting this form into (14.20) with (14.21) and cancelling $e^{\lambda t}$, we get, for each k,

$$\begin{aligned} \lambda\mathbf{W}_k &= \gamma A\mathbf{W}_k + D\nabla^2\mathbf{W}_k \\ &= \gamma A\mathbf{W}_k - Dk^2\mathbf{W}_k . \end{aligned}$$

We require nontrivial solutions for $\mathbf{W}_k$ so the λ are determined by the roots of the characteristic polynomial

$$|\lambda I - \gamma A + Dk^2| = 0 .$$

Evaluating the determinant with A and D from (14.15) and (14.20) we get the eigenvalues $\lambda(k)$ as functions of the wavenumber k as the roots of

$$\begin{aligned} &\lambda^2 + \lambda[k^2(1+d) - \gamma(f_u + g_v)] + h(k^2) = 0 , \\ &h(k^2) = dk^4 - \gamma(df_u + g_v)k^2 + \gamma^2|A| . \end{aligned} \tag{14.23}$$

The steady state (u_0, v_0) is linearly stable if both solutions of (14.23) have $\mathrm{Re}\,\lambda < 0$. We have already imposed the constraints that the steady state is stable in the absence of any spatial effects, that is $\mathrm{Re}\,\lambda(k^2 = 0) < 0$. The quadratic (14.23) in this case is (14.17) and the requirement that $\mathrm{Re}\,\lambda < 0$ gave conditions (14.19). For the steady state to be unstable to *spatial* disturbances we require $\mathrm{Re}\,\lambda(k) > 0$ for some $k \neq 0$. This can happen if either the coefficient of λ in (14.23) is negative, or if $h(k^2) < 0$ for some $k \neq 0$. Since $(f_u + g_v) < 0$ from conditions (14.19) and $k^2(1+d) > 0$ for all $k \neq 0$ the coefficient of λ, namely

$$[-\gamma(f_u + g_v) + k^2(1+d)] > 0 ,$$

so the only way $\mathrm{Re}\,\lambda(k^2)$ can be positive is if $h(k^2) < 0$ for some k. This is immediately clear from the solutions of (14.23), namely

$$2\lambda = [k^2(1+d) - \gamma(f_u + g_v)] \pm \{[k^2(1+d) - \gamma(f_u + g_v)]^2 - 4h(k^2)\}^{1/2} .$$

Since we required the determinant $|A| > 0$ from (14.19) the only possibility for $h(k^2)$ in (14.23) to be negative is if $(df_u + g_v) > 0$. Since $(f_u + g_v) < 0$ from (14.19) this implies that $d \neq 1$ and f_u and g_v must have opposite signs. So, a further requirement to those in (14.19) is

$$df_u + g_v > 0 \quad \Rightarrow \quad d \neq 1 . \tag{14.24}$$

With the reaction kinetics giving the null clines in Fig. 14.2 we noted that $f_u > 0$ and $g_v < 0$, so the first condition in (14.19) and the last inequality require that the diffusion coefficient ratio $d > 1$. For example, in terms of the activator-inhibitor mechanism (14.8) this means that the inhibitor must diffuse faster than the activator as we noted above.

The last inequality is necessary but not sufficient for $\mathrm{Re}\,\lambda > 0$. For $h(k^2)$ to be negative for some non-zero k, the minimum $h_{\min}$ must be negative. From (14.23), elementary differentiation with respect to k^2 shows that

$$h_{\min} = \gamma^2\left[|A| - \frac{(df_u + g_v)^2}{4d}\right], \quad k^2 = k_m^2 = \gamma\frac{df_u + g_v}{2d} . \tag{14.25}$$

Thus the condition that $h(k^2) < 0$ for some $k^2 \neq 0$ is

$$\frac{(df_u + g_v)^2}{4d} > |A| . \tag{14.26}$$

At bifurcation, when $h_{\min} = 0$, we require $|A| = (df_u + g_v)^2/4d$ and so for fixed kinetics parameters this defines a critical diffusion coefficient ratio $d_c(> 1)$ as the appropriate root of

$$d_c^2 f_u^2 + 2(2f_v g_u - f_u g_v)d_c + g_v^2 = 0 \,. \tag{14.27}$$

The critical wavenumber k_c is then given by

$$k_c^2 = \gamma \frac{d_c f_u + g_v}{2d_c} = \gamma \left[\frac{|A|}{d_c}\right]^{1/2} = \gamma \left[\frac{f_u g_v - f_v g_u}{d_c}\right]^{1/2} . \tag{14.28}$$

Fig. 14.4 (a) shows how $h(k^2)$ varies as a function of k^2 for various d.

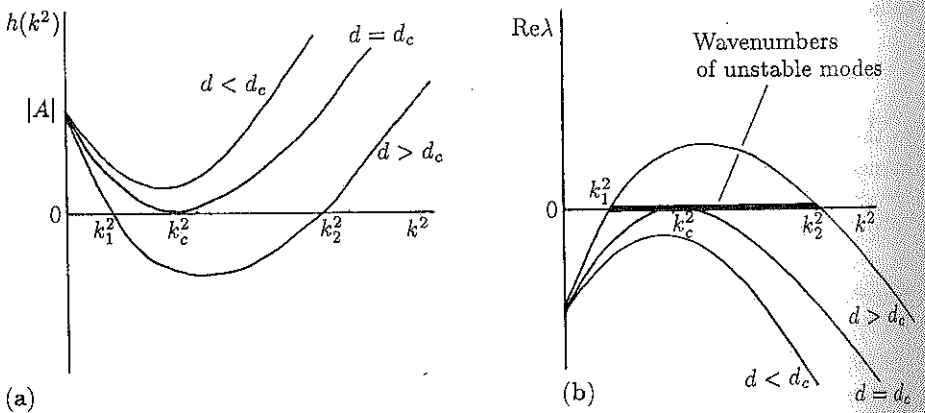

Fig. 14.4a,b. (a) Plot of $h(k^2)$ defined by (14.23) for typical kinetics illustrated in Fig. 14.2. When the diffusion coefficient ratio d increases beyond the critical value d_c, $h(k^2)$ becomes negative for a finite range of $k^2 > 0$. (b) Plot of the largest of the eigenvalues $\lambda(k^2)$ from (14.23) as a function of k^2. When $d > d_c$ there is a range of wavenumbers $k_1^2 < k^2 < k_2^2$ which are linearly unstable.

Whenever $h(k^2) < 0$, (14.23) has a solution λ which is positive for the same range of wavenumbers that make $h < 0$. From (14.23) with $d > d_c$ the range of unstable wavenumbers $k_1^2 < k^2 < k_2^2$ is obtained from the zeros k_1^2 and k_2^2 of $h(k^2) = 0$ as

$$\begin{aligned} k_1^2 &= \gamma \frac{(df_u + g_v) - \{(df_u + g_v)^2 - 4d|A|\}^{1/2}}{2d} < k^2 \\ &< \gamma \frac{(df_u + g_v) + \{(df_u + g_v)^2 - 4d|A|\}^{1/2}}{2d} = k_2^2 \,. \end{aligned} \tag{14.29}$$

Fig. 14.4 (b) plots a typical $\lambda(k^2)$ against k^2. The expression $\lambda = \lambda(k^2)$ is called a *dispersion relation*. We discuss the importance and use of dispersion relations

in more detail in the next two sections. Note that, within the unstable range, $\mathrm{Re}\,\lambda(k^2) > 0$ has a maximum for the wavenumber k_m obtained from (14.25) with $d > d_c$. This implies that there is a fastest growing mode in the summation (14.22) for w; this is an attribute we shall now exploit.

If we consider the solution w given by (14.22), the dominant contributions as t increases are those modes for which $\mathrm{Re}\,\lambda(k^2) > 0$ since all other modes tend to zero exponentially. From Fig. 14.4, or analytically from (14.29), we determine the range, $k_1^2 < k^2 < k_2^2$ where $h(k^2) < 0$, and hence $\mathrm{Re}\,\lambda(k^2) > 0$, and so from (14.22)

$$\mathbf{w}(\mathbf{r}, t) \sim \sum_{k_1}^{k_2} c_k \exp[\lambda(k^2)t]\mathbf{W}_k(\mathbf{r}) \quad \text{for large } t \,. \tag{14.30}$$

An analysis and graph of the dispersion relation are thus extremely informative in that they immediately say which eigenfunctions, that is which spatial patterns, are linearly unstable and grow exponentially with time. We must keep in mind that, with finite domain eigenvalue problems, the wavenumbers are discrete and so only certain k in the range (14.29) are of relevance: we discuss the implications of this later.

The key assumption, and what in fact happens, is that these linearly unstable eigenfunctions in (14.30) which are growing exponentially with time will eventually be bounded by the nonlinear terms in the reaction diffusion system of equations and an ultimate steady state spatially inhomogeneous solution will emerge. A key element in this assumption is the existence of a confined set for the kinetics (see Chapter 3). We would intuitively expect that if a confined set exists for the kinetics, the same set would also contain the solutions when diffusion is included. This is indeed the case and can be rigorously proved; see Smoller (1983). So, part of the analysis of a specific mechanism involves the demonstration of a confined set within the *positive* quadrant. A general nonlinear analysis for the evolution to the finite amplitude steady state spatial patterns is still lacking but singular perturbation analyses for d near the bifurcation value d_c have been carried out and a non-uniform spatially heterogeneous solution is indeed obtained (see, for example, Lara and Murray 1983; an early nonlinear analysis of a predator-prey system was given by Segel and Levin 1976). There have been many spatially inhomogeneous solutions evaluated numerically using a variety of specific reaction diffusion mechanisms. The results presented in the next chapter illustrate some of the richness of pattern which can be generated.

To recap, we have now obtained conditions for the generation of spatial patterns by *two*-species reaction diffusion mechanisms of the form (14.11). For convenience we reproduce them here. Remembering that all derivatives are evaluated at the steady state (u_0, v_0), they are, from (14.19), (14.24), (14.26),

$$\begin{aligned} &f_u + g_v < 0, \quad f_u g_v - f_v g_u > 0 \,, \\ &df_u + g_v > 0, \quad (df_u + g_v)^2 - 4d(f_u g_v - f_v g_u) > 0 \,. \end{aligned} \tag{14.31}$$

The derivatives f_u and g_v must be of opposite sign: with the reaction kinetics

exhibited in Fig. 14.2, $f_u > 0$, $g_v < 0$ so the first and third of (14.31) imply that the ratio of diffusion coefficients $d > 1$. If the conditions (14.31) are satisfied there is a scale(γ)-dependent range of patterns, with wavenumbers defined by (14.29), which are linearly unstable. The spatial patterns which initially grow (exponentially) are those eigenfunctions $\mathbf{W}_k(\mathbf{r})$ with wavenumbers k_1 and k_2 determined by (14.29); namely those in (14.30). Note that the scale parameter γ plays a crucial role in these expressions, a point we consider further in the next section. Generally we would expect the kinetics and morphogen diffusion coefficients to be fixed. The only natural variable parameter is then γ which reflects the size of the embryo or rather the embryonic domain we are considering.

Diffusion Driven Instability in Infinite Domains: Continuous Spectrum of Eigenvalues

In a finite domain the possible wavenumbers k and corresponding spatial wavelengths of allowable patterns are discrete and depend in part on the boundary conditions. In developmental biology the size of the embryo during the period of spatial patterning is often sufficiently large, relative to the pattern to be formed, that the 'boundaries' cannot play a major role in isolating specific wavelengths, as for example in the generation of patterns of hair, scale and feather primordia (see Chapter 17). Thus, for practical purposes the pattern formation domain is effectively infinite. Here we describe how to determine the spectrum of unstable eigenvalues for an infinite domain – it is considerably easier than for a finite domain.

We start with the linearised system (14.20) and look for solutions in the form

$$\mathbf{w}(\mathbf{r},t) \propto \exp\left[\lambda t + i\mathbf{k}\cdot\mathbf{r}\right],$$

where $\mathbf{k}$ is the wave vector with magnitude $k = |\mathbf{k}|$. Substitution into (14.20) again gives

$$|\lambda I - \gamma A + Dk^2| = 0$$

and so the dispersion relation giving λ in terms of the wavenumbers k is again given by (14.23). The range of eigenvalues for which $\mathrm{Re}\,\lambda(k^2) > 0$ is again given by (14.29). The crucial difference between the situation here and that for a finite domain is that there is always a spatial pattern if, in (14.29), $0 < k_1^2 < k_2^2$ since we are not restricted to a discrete class of k^2 defined by the eigenvalue problem (14.21). So at bifurcation when k_c^2, given by (14.28), is linearly unstable the mechanism will evolve to a spatial pattern with the critical wavelength $\omega_c = 2\pi/k_c$. Thus the wavelength with the maximum exponential growth in Fig. 14.4(b) will be the pattern which generally emerges. In the next chapter on biological applications we shall see that the difference between a finite domain and an effectively infinite one has important biological implications: finite domains put considerable restrictions on the allowable patterns.

14.4 Detailed Analysis of Pattern Initiation in a Reaction Diffusion Mechanism

Here we consider a specific two-species reaction diffusion system and carry out the detailed analysis. We lay the groundwork in this section for the subsequent applications to real biological pattern formation problems. We calculate the eigenfunctions, obtain the specific conditions on the parameters necessary to initiate spatial patterns and determine the wavenumbers and wavelengths of the spatial disturbances which initially grow exponentially.

We study the simplest reaction diffusion mechanism (14.7), first in one space dimension, namely

$$\begin{aligned} u_t &= \gamma f(u,v) + u_{xx} = \gamma(a - u + u^2 v) + u_{xx}\,, \\ v_t &= \gamma g(u,v) + d v_{xx} = \gamma(b - u^2 v) + d v_{xx}\,. \end{aligned} \tag{14.32}$$

The kinetics null clines $f = 0$ and $g = 0$ are illustrated in Fig. 14.2 (a). The uniform positive steady state (u_0, v_0) is

$$u_0 = a + b, \quad v_0 = \frac{b}{(a+b)^2}, \quad b > 0, \quad a + b > 0 \tag{14.33}$$

and, at the steady state,

$$\begin{aligned} &f_u = \frac{b-a}{a+b}, \quad f_v = (a+b)^2 > 0, \quad g_u = \frac{-2b}{a+b}\,, \\ &g_v = -(a+b)^2 < 0, \quad f_u g_v - f_v g_u = (a+b)^2 > 0\,. \end{aligned} \tag{14.34}$$

Since f_u and g_v must have opposite signs we must have $b > a$. With these expressions, conditions (14.31) require

$$\begin{aligned} &f_u + g_v < 0 \quad \Rightarrow \quad 0 < b - a < (a+b)^3\,, \\ &f_u g_v - f_v g_u > 0 \quad \Rightarrow \quad (a+b)^2 > 0\,, \\ &d f_u + g_v > 0 \quad \Rightarrow \quad d(b-a) > (a+b)^3\,, \\ &(d f_u + g_v)^2 - 4d(f_u g_v - f_v g_u) > 0 \\ &\Rightarrow \quad [d(b-a) - (a+b)^3]^2 > 4d(a+b)^4\,. \end{aligned} \tag{14.35}$$

These inequalities define a domain in (a, b, d) parameter space, called the *Turing space*, within which the mechanism will be unstable to certain spatial disturbances of given wavenumbers k, which we now determine.

Consider the related eigenvalue problem (14.21) and let us choose the domain to be $x \in (0, p)$ with $p > 0$. We then have

$$\mathbf{W}_{xx} + k^2 \mathbf{W} = 0, \quad \mathbf{W}_x = 0 \text{ for } x = 0, p \tag{14.36}$$

the solutions of which are

$$\mathbf{W}_n(x) = \mathbf{A}_n \cos(n\pi x/p), \quad n = \pm 1, \pm 2, \ldots \tag{14.37}$$

where the $\mathbf{A}_n$ are arbitrary constants. The eigenvalues are the *discrete* wavenumbers $k = n\pi/p$. Whenever (14.34) are satisfied and there is a range of wavenumbers $k = n\pi/p$ lying within the bound defined by (14.29), then the corresponding eigenfunctions $\mathbf{W}_n$ are linearly unstable. Thus the eigenfunctions (14.37) with wavelengths $\omega = 2\pi/k = 2p/n$ are the ones which initially grow with time like $\exp\{\lambda([n\pi/p]^2)t\}$. The band of wavenumbers from (14.29), with (14.34), is given by

$$\gamma L(a,b,d) = k_1^2 < k^2 = \left(\frac{n\pi}{p}\right)^2 < k_2^2 = \gamma M(a,b,d)$$

$$L = \frac{([d(b-a)-(a+b)^3] - \{[d(b-a)-(a+b)^3]^2 - 4d(a+b)^4\}^{1/2}}{2d(a+b)},$$

$$M = \frac{([d(b-a)-(a+b)^3] + \{[d(b-a)-(a+b)^3]^2 - 4d(a+b)^4\}^{1/2}}{2d(a+b)}. \tag{14.38}$$

In terms of the wavelength $\omega = 2\pi/k$, the range of unstable modes $\mathbf{W}_n$ have wavelengths bounded by ω_1 and ω_2 where

$$\frac{4\pi^2}{\gamma L(a,b,d)} = \omega_1^2 > \omega^2 = \left(\frac{2p}{n}\right)^2 > \omega_2^2 = \frac{4\pi^2}{\gamma M(a,b,d)}. \tag{14.39}$$

Note in (14.38) the importance of scale, quantified by γ. The smallest wavenumber is π/p, that is $n = 1$. For fixed parameters a, b and d, if γ is sufficiently small (14.38) says that there is *no allowable* k in the range, and hence no mode $\mathbf{W}_n$ in (14.37), which can be driven unstable. This means that all modes in the solution $\mathbf{w}$ in (14.30) tend to zero exponentially and the steady state is stable. We discuss this important role of scale in more detail below.

From (14.30) the spatially heterogeneous solution which emerges is the sum of the unstable modes, namely

$$\mathbf{w}(x,t) \sim \sum_{n_1}^{n_2} \mathbf{C}_n \exp\left[\lambda\left(\frac{n^2\pi^2}{p^2}\right)t\right] \cos\frac{n\pi x}{p} \tag{14.40}$$

where λ is given by the positive solution of the quadratic (14.23) with the derivatives from (14.34), n_1 is the smallest integer greater than or equal to pk_1/π, n_2 the largest integer less than or equal to pk_2/π and $\mathbf{C}_n$ are constants which are determined by a Fourier series analysis of the initial conditions for $\mathbf{w}$. Initial conditions in any biological context involve a certain stochasticity and so it is inevitable that the Fourier spectrum will contain the whole range of Fourier modes, that is the $\mathbf{C}_n$ are non-zero. We can therefore assume at this stage that

γ is sufficiently large to ensure that allowable wavenumbers exist in the unstable range of k. Before discussing the possible patterns which emerge let us first obtain the corresponding two-dimensional result.

Consider the two-dimensional domain defined by $0 < x < p$, $0 < y < q$ whose rectangular boundary we denote by ∂B. The spatial eigenvalue problem in place of that in (14.36) is now

$$\nabla^2\mathbf{W} + k^2\mathbf{W} = 0, \quad (\mathbf{n}\cdot\nabla)\mathbf{W} = 0 \quad \text{for} \quad (x,y) \text{ on } \partial B \tag{14.41}$$

the eigenfunctions of which are

$$\mathbf{W}_{p,q}(x,y) = \mathbf{C}_{n,m} \cos\frac{n\pi x}{p} \cos\frac{m\pi y}{q}, \quad k^2 = \pi^2\left(\frac{n^2}{p^2} + \frac{m^2}{q^2}\right), \tag{14.42}$$

where n and m are integers. The two-dimensional modes $\mathbf{W}_k(x,y)$ which are linearly unstable are those with wavenumbers k, defined by the last equation, lying within the unstable band of wavenumbers defined in terms of a, b and d by (14.38). We again assume that γ is sufficiently large so that the range of unstable wavenumbers contains at least one possible mode. Now the unstable spatially patterned solution is given by (14.30) with (14.42) as

$$\mathbf{w}(x,y,t) \sim \sum_{n,m} \mathbf{C}_{n,m} \exp[\lambda(k^2)t] \cos\frac{n\pi x}{p} \cos\frac{m\pi y}{q},$$

$$\gamma L(a,b,d) = k_1^2 < k^2 = \pi^2\left(\frac{n^2}{p^2} + \frac{m^2}{q^2}\right) < k_2^2 = \gamma M(a,b,d), \tag{14.43}$$

where the summation is over all pairs (n,m) which satisfy the inequality, L and M are defined by (14.38) as before and $\lambda(k^2)$ is again the positive solution of (14.23) with the expressions for the derivatives of f and g given by (14.34). As t increases a spatial pattern evolves which is initially made up of the modes in (14.43).

Now consider the type of spatial patterns we might expect from the unstable solutions in (14.40) and (14.43). Suppose first that the domain size, as measured by γ, is such that the range of unstable wavenumbers in (14.38) admits only the wavenumber $n = 1$: the corresponding dispersion relation for λ in terms of the wavelengths $\omega = 2p/n$, is illustrated in Fig. 14.5 (a) below. The only unstable mode, from (14.37) is then $\cos(\pi x/p)$ and the growing instability is given by (14.40) as

$$\mathbf{w}(x,t) \sim \mathbf{C}_1 \exp\left[\lambda\left(\frac{\pi^2}{p^2}\right)t\right] \cos\frac{\pi x}{p},$$

where λ is the positive root of the quadratic (14.23) with f_u, f_v, g_u and g_v from (14.34) and with $k^2 = (\pi/p)^2$. Here all other modes decay exponentially with time. We can only determine the $\mathbf{C}_1$ from initial conditions. To get an intuitive understanding for what is going on, let us simply take $\mathbf{C}_1$ as $(\varepsilon, \varepsilon)$ for some small

positive ε and consider the morphogen u; that is from the last equation and the definition of w from (14.14),

$$u(x,t) \sim u_0 + \varepsilon \exp\left[\lambda\left(\frac{\pi^2}{p^2}\right)t\right]\cos\frac{\pi x}{p}\,. \tag{14.44}$$

This unstable mode, which is the dominant solution which emerges as t increases, is illustrated in Fig. 14.5 (b). In other words, this is the pattern predicted by the dispersion relation in Fig. 14.5 (a).

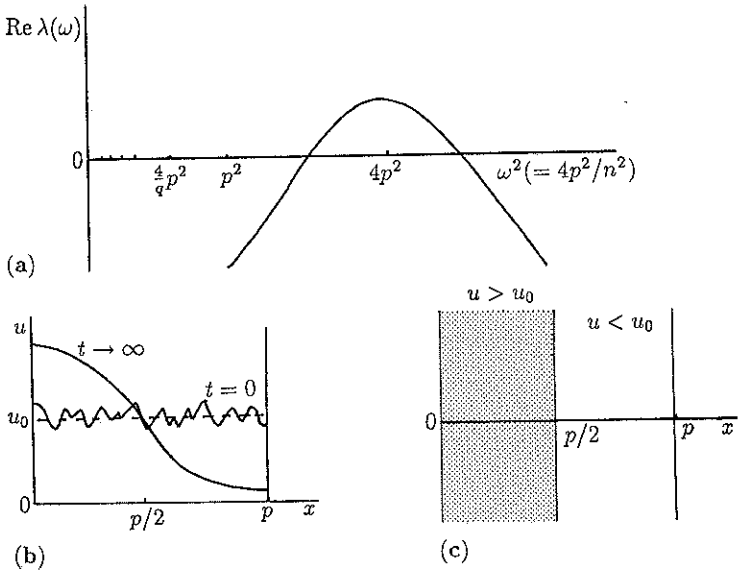

Fig. 14.5a-c. (a) Typical dispersion relation for the growth factor $\mathrm{Re}\,\lambda$ as a function of the wavelength ω obtained from a linearisation about the steady state. The only mode which is linearly unstable has $n = 1$; all other modes have $\mathrm{Re}\,\lambda < 0$. (b) The temporally growing linear mode which eventually evolves from random initial conditions into a finite amplitude spatial pattern such as shown in (c), where the shaded area corresponds to a concentration higher than the steady state u_0 and the unshaded area to a concentration lower than the steady state value.

Clearly if the exponentially growing solution was valid for all time it would imply $u \to \infty$ as $t \to \infty$. For the mechanism (14.32) the kinetics has a confined set, within the positive quadrant, which bounds the solution. So the solution in the last equation must be bounded and lie in the positive quadrant. We hypothesise that this growing solution eventually settles down to a spatial pattern which is similar to the single cosine mode shown in Fig. 14.5 (b). As mentioned before, singular perturbation analyses in the vicinity of the bifurcation in one of the parameters, for example near the critical domain size for γ such that a single

wavenumber is just unstable, or when the critical diffusion coefficient ratio is near d_c, bear this out as do the many numerical simulations of the full nonlinear equations. Fig. 14.5 (c) is a useful way of presenting spatial patterned results for reaction diffusion mechanisms – the shaded region represents a concentration above the steady state value while the unshaded region represents concentrations below the steady state value. As we shall see, this simple way of presenting the results is very useful in the application of chemical prepattern theory to patterning problems in developmental biology, where it is postulated that cells differentiate when one of the morphogen concentrations is above (or below) some threshold level.

Let us now suppose that the domain size is doubled, say. With the definition of γ chosen to represent scale this is equivalent to multiplying the original γ by 4 since in the one-dimensional situation $\sqrt{\gamma}$ is proportional to size, that is length, of the domain. This means that the dispersion relation and the unstable range are simply moved along the k^2-axis or along the ω^2-axis. Suppose the original $\gamma = \gamma_1$. The inequalities (14.38) determine the unstable modes as those with wavelengths $\omega(= 2\pi/k)$ determined by (14.39), namely

$$\frac{4\pi^2}{\gamma_1 L(a,b,d)} > \omega^2 > \frac{4\pi^2}{\gamma_1 M L(a,b,d)}\,. \tag{14.45}$$

Let this be the case illustrated in Fig. 14.5 (a) and which gave rise to the pattern in Fig. 14.5 (c). Now let the domain double in size. We consider exactly the same domain as in Fig. 14.5 but with an increased γ to $4\gamma_1$. This is equivalent to having the same γ_1 but with a domain 4 times that in Fig. 14.5. We choose the former means of representing a change in scale. The equivalent dispersion relation is now illustrated in Fig. 14.6 (a) – it is just the original one of Fig. 14.5 (a) moved along so that the wavelength of the excited or unstable mode now has $\omega = p$, that is $n = 2$. The equivalent spatial pattern is then as in Fig. 14.6 (b). As we shall see in the applications chapter which follows, it is a particularly convenient way, when presenting spatial patterned solutions, to incorporate scale solely via a change in γ.

We can thus see with this example how the patterning process works as regards domain size. There is a basic wavelength picked out by the analysis for a given $\gamma = \gamma_1$, in this example that with $n = 1$. As the domain grows it eventually can incorporate the pattern with $n = 2$ and progressively higher modes the larger the domain, as shown in Fig. 14.6 (c). In the same way if the domain is sufficiently small there is clearly a $\gamma = \gamma_c$ such that the dispersion relation, now moved to the right in Fig. 14.6 (a), will not even admit the wavelength with $n = 1$. In this case no mode is unstable and so no spatial pattern can be generated. The concept of a critical domain size for the existence of spatial pattern is an important one both in developmental biology, and in spatially dependent ecological models as we shall see later.

Note in Fig. 14.6 (b) the two possible solutions for the same parameters and zero flux boundary conditions. Which of these is obtained depends on the bias in the inital conditions. Their existence poses certain conceptual difficulties

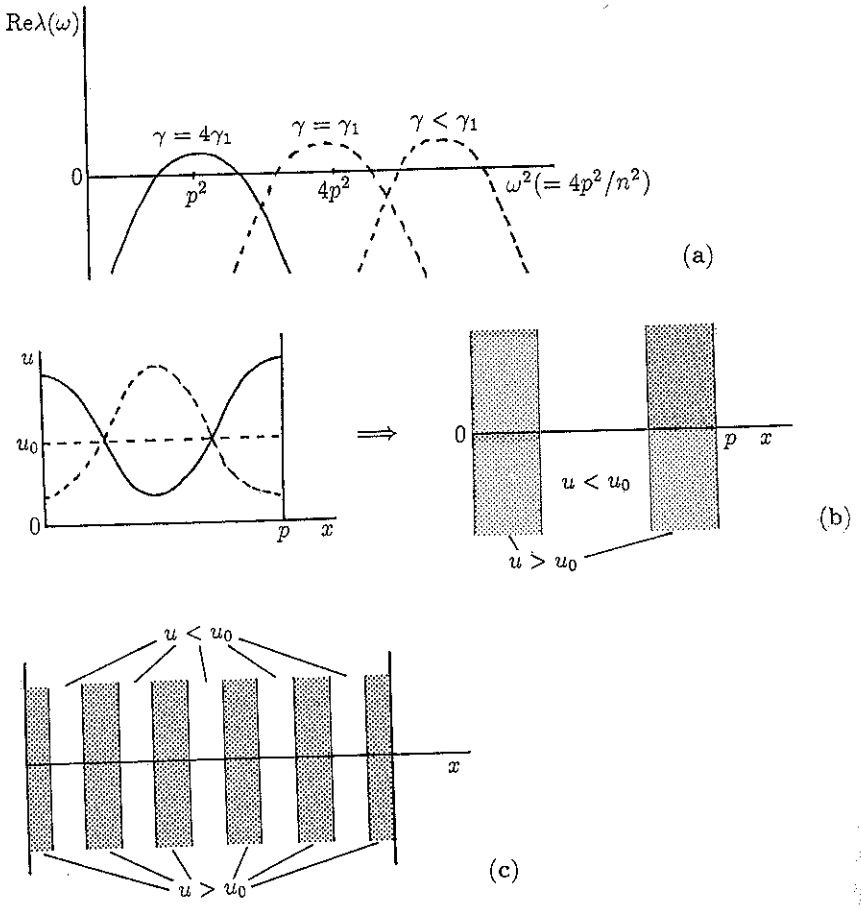

Fig. 14.6a-c. (a) Dispersion relation Re λ as a function of the wavelength ω when the single mode with $n = 2$ is unstable for a domain size $4\gamma_1$; the dashed curves are those with $\gamma = \gamma_1$ and $\gamma < \gamma_c < \gamma_1$ where γ_c is the scale value of the domain that will not admit any heterogeneous pattern. (b) The spatial pattern in the morphogen u predicted by the dispersion relation in (a). The dashed line, the mirror image about $u = u_0$ is also an allowable form of this solution. The initial conditions determine which pattern is obtained. (c) The spatial pattern obtained when the domain is sufficiently large to fit in the number of unstable modes equivalent to $n = 10$: the shaded regions represent morphogen levels $u > u_0$, the uniform steady state.

from a developmental biology point of view within the context of positional information. If cells differentiate when the morphogen concentration is larger than some threshold then the differentiated cell pattern is obviously different for each of the two possible solutions. Development, however, is a sequential process and so a previous stage generally cues the next. In the context of reaction diffusion models this implies a bias in the initial conditions towards one of the patterns.

Now consider the two-dimensional problem with a dispersion relation such that the unstable modes are given by (14.43). Here the situation is not so

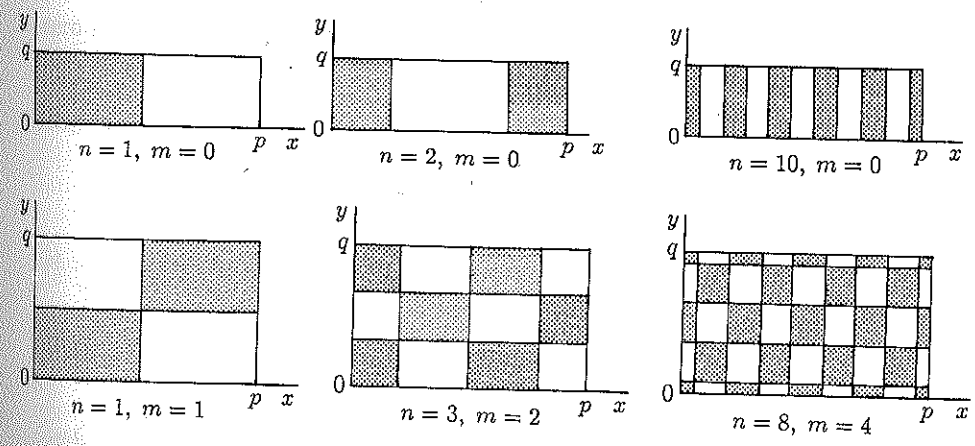

Fig. 14.7. Typical two-dimensional spatial patterns indicated by the linearly unstable solution (14.43) when various wavenumbers are in the unstable range. The shaded regions are where $u > u_0$, the uniform steady state.

straightforward since for a given γ, representing the *scale*, the actual modes which are unstable now depend on the domain *geometry* as measured by the length p and the width q. Referring to (14.43), first note that if the width is sufficiently small, that is q is small enough, even the first mode with $m = 1$ lies outside the unstable range. The problem is then equivalent to the above one-dimensional situation. As the width increases, that is q increases, genuine two-dimensional modes with $n \neq 0$ and $m \neq 0$ become unstable since $\pi^2(n^2/p^2 + m^2/q^2)$ lies in the range of unstable wavenumbers. Fig. 14.7 illustrates typical temporally growing spatial patterns indicated by (14.43) with various non-zero n and m.

Regular Planar Tesselation Patterns

The linear patterns illustrated in the last figure arise from the simplest two-dimensional eigenfunctions of (14.41). Less simple domains require the solutions of

$$\nabla^2\psi + k^2\psi = 0, \quad (\mathbf{n}\cdot\nabla)\psi = 0 \quad \text{for} \quad \mathbf{r} \text{ on } \partial B\,. \tag{14.46}$$

Except for simple geometries the analysis quickly becomes quite complicated. Even for circular domains the eigenvalues have to be determined numerically. Surprisingly, there are some elementary solutions for symmetric domains which tesselate the plane, namely squares, hexagons, rhombi and, by subdivision, triangles: these were found by Christopherson (1940). In other words we can cover the complete plane with, for example, regular hexagonal tiles. [The basic symmetry group of regular polygons are hexagons, squares and rhombi, with, of course, triangles, which are subunits of these.] Thus we want solutions ψ where the unit cell, with zero flux conditions on its boundary, is one of the regular tesselations which can cover the plane. That is we want solutions which are *cell* periodic: the

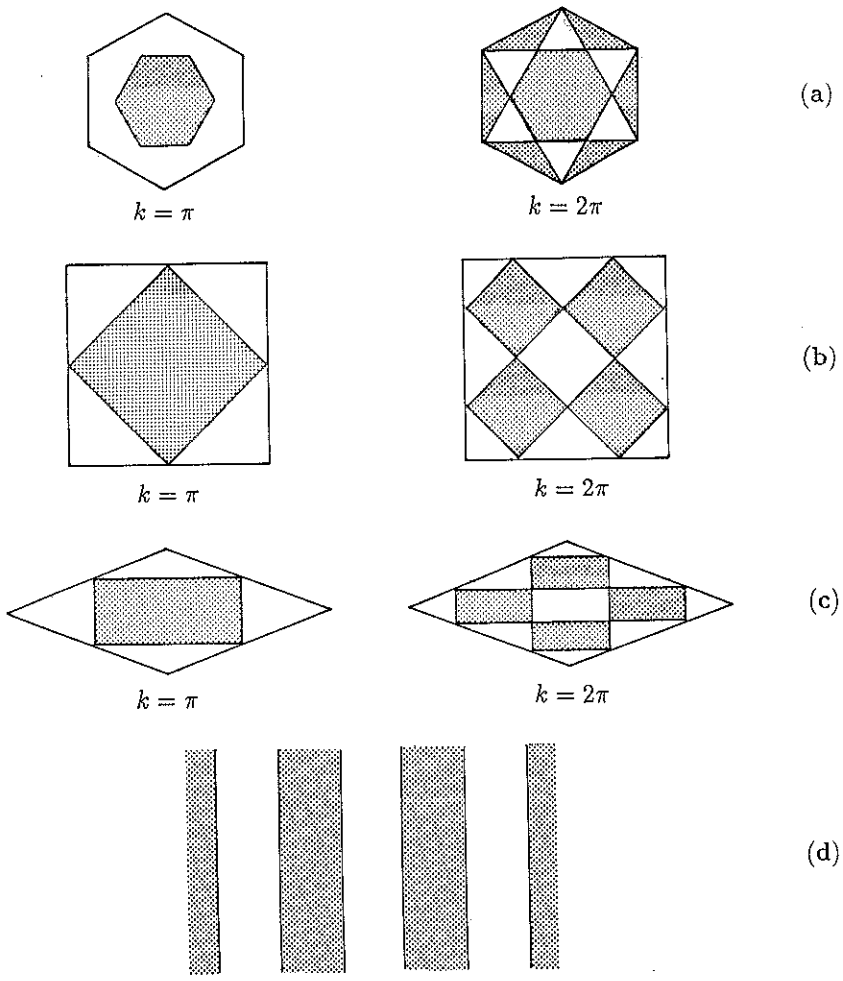

Fig. 14.8a-d. (a) Patterns which are obtained with the solution (14.47) with $k = \pi$ and $k = 2\pi$. The shaded region is where $\psi > 0$ and the unshaded region where $\psi < 0$. (b) Patterns generated by the solution (14.48) for a square tesselation with $k = \pi$ and $k = 2\pi$. (c) Rhombic patterns from (14.49) with $k = \pi$ and $k = 2\pi$. (d) One-dimensional roll patterns from (14.50).

word 'cell' is, of course, here meant as the unit of tesselation.

The solution of (14.46) for a hexagon is

$$\psi(x,y) = \frac{\cos k\left(\frac{\sqrt{3}y}{2} + \frac{x}{2}\right) + \cos k\left(\frac{\sqrt{3}y}{2} - \frac{x}{2}\right) + \cos kx}{3}$$
$$= \frac{\cos\left\{kr\sin\left(\theta + \frac{\pi}{6}\right)\right\} + \cos\left\{kr\sin\left(\theta - \frac{\pi}{6}\right)\right\} + \cos\left\{kr\sin\left(\theta - \frac{\pi}{2}\right)\right\}}{3}, \tag{14.47}$$

From (14.46), ψ is independent to the extent of multiplication by an arbitrary

constant: the form chosen here makes $\psi = 1$ at the origin. This solution satisfies zero flux boundary conditions on the hexagonal symmetry boundaries if $k = n\pi$, $n = \pm 1, \pm 2, \ldots$ Fig. 14.8 (a) shows the type of pattern the solution can generate.

The polar coordinate form shows the invariance to hexagonal rotation, that is invariance to rotation by $\pi/3$, as it must. That is

$$\psi(r,\theta) = \psi(r,\theta + \frac{\pi}{3}) = H\psi(r,\theta) = \psi(r,\theta)\ ,$$

where H is the hexagonal rotation operator.

The solution for the square is

$$\psi(x,y) = \frac{\cos kx + \cos ky}{2}$$
$$= \frac{\cos(kr\cos\theta) + \cos(kr\sin\theta)}{2}\ , \tag{14.48}$$

where $k = \pm 1, \pm 2 \ldots$ and $\psi(0,0) = 1$. This solution is square rotationally invariant since

$$\psi(r,\theta) = \psi(r,\theta + \frac{\pi}{2}) = S\psi(r,\theta) = \psi(r,\theta)\ ,$$

where S is the square rotational operator. Typical patterns are illustrated in Fig. 14.8 (b).

The solution for the rhombus is

$$\psi(x,y) = \frac{\cos kx + \cos\{k(x\cos\phi + y\sin\phi)\}}{2}$$
$$= \frac{\cos\{kr\cos\theta\} + \cos\{k(r\cos(\theta - \phi)\}}{2}\ , \tag{14.49}$$

where ϕ is the rhombus angle and again $k = \pm 1, \pm 2, \ldots$ This solution is invariant under a rhombic rotation, that is

$$\psi(r,\theta;\phi) = \psi(r,\theta + \pi;\phi) = R\psi(r,\theta;\phi)\ ,$$

where R is the rhombic rotation operator. Illustrative patterns are shown in Fig. 14.8 (c).

A further cell periodic solution is the one-dimensional version of the square; that is there is only variation in x. The solutions here are of the form

$$\psi(x,y) = \cos kx, \quad k = n\pi, \quad n = \pm 1, \pm 2, \ldots \tag{14.50}$$

and represent rolls with patterns as in Fig. 14.8 (d). These, of course, are simply the one-dimensional solutions (14.37).

When the full nonlinear equations are solved numerically with initial conditions taken to be small random perturbations about the steady state, linear

theory turns out to be a good predictor of the ultimate steady state in the one-dimensional situation, particularly if the unstable modes have large wavelengths, that is small wavenumbers. With larger wavenumbers the predictions are less reliable – and even more so with two-dimensional structures. Since the equations we have studied are linear and invariant when multiplied by a constant, we can have equivalent solutions which are simply mirror images in the line $u = u_0$: refer to Fig. 14.6 (b). Thus the pattern that evolves depends on the initial conditions and the final pattern tends to be the one closest to the initial conditions. There is, in a sense, a basin of attraction for the spatial patterns as regards the initial conditions. Once again near bifurcation situations singular perturbation analysis indicates nonlinear patterns closely related to the linear predictions. In general, however, away from the bifurcation boundaries linear predictions are much less reliable: see the computed patterns exhibited in the next chapter. Except for the simplest patterns, we should really use linear theory for two and three dimensions only as a guide to the wealth of patterns which can be generated by pattern formation mechanisms. Linear theory does however determine the parameter ranges for pattern generation.

The application of reaction diffusion pattern generation to specific developmental biology problems is usually within the context of a prepattern theory whereby cells differentiate according to the level of the morphogen concentration. If the spatial pattern is quite distinct, that is with relatively large gradients, less sensitive tuning is required of the cells in order to carry out their assigned roles than if the pattern variation or the concentration gradients are small. It is useful therefore to try to get a quantitative measure of spatial heterogeneity, which is meaningful biologically, so as to compare different mechanisms. Another biologically relevant method will be discussed in the next section.

Berding (1987) introduced a 'heterogeneity' function for the spatial patterns generated by reaction diffusion systems with zero flux boundary conditions. Suppose the general mechanism (14.10), in one space variable, is diffusionally unstable and the solutions evolve to the spatially inhomogeneous steady state solutions $U(x)$ and $V(x)$ as $t \to \infty$. With the definition of γ in (14.6) proportional to the square of the domain length we can measure domain size by γ and hence take x to be in (0,1). Then (U, V) satisfy the dimensionless equations

$$U'' + \gamma f(U,V) = 0, \quad dV'' + \gamma g(U,V) = 0\,, \qquad (14.51)$$
$$U'(0) = U'(1) = V'(0) = V'(1) = 0\,.$$

The non-negative heterogeneity function is defined by

$$H = \int_0^1 (U'^2 + V'^2)\,dx \geq 0\,, \qquad (14.52)$$

which depends only on the parameters of the system and the domain scale γ. H

conditions in (14.51),

$$H = -\int_0^1 (UU'' + VV'')\,dx$$

which, on using (14.51) for U'' and V'', becomes

$$H = \frac{\gamma}{d}\int_0^1 [dUf(U,V) + Vg(U,V)]\,dx\,. \qquad (14.53)$$

If there is no spatial patterning, U and V are simply the uniform steady state solutions of $f(U,V) = g(U,V) = 0$ and so $H = 0$, as also follows, of course, from the definition (14.52).

From (14.53) we see how the scale parameter and diffusion coefficient ratio appear in the definition of heterogeneity. For example, suppose the domain is such that it sustains a single wave for $\gamma = \gamma_1$, in dimensional terms a domain length $L = L_1$ say. If we then double the domain size to $2L_1$ we can fit in two waves and so, intuitively from (14.52), H must increase as there is more heterogeneity. Since $\gamma \propto L^2$, H from (14.53) is simply quadrupled. From an embryological point of view, for example, this means that as the embryo grows we expect more and more structure. An example of this increase in structure in a growing domain is illustrated in Fig. 14.15 below. Berding (1987) discusses particular applications and compares specific reaction diffusion mechanisms as regards their potential for heterogeneity.

14.5 Dispersion Relation, Turing Space, Scale and Geometry Effects in Pattern Formation in Morphogenetic Models

We first note some general properties about the dispersion relation and then exploit it further with the specific case we analysed in the last section. The formation of spatial patterns by any morphogenetic model is principally a nonlinear phenomenon. However, as we noted, a good indication of the patterns in one dimension can be obtained by a simple linear analysis. For spatial patterns to form, we saw that two conditions must hold simultaneously. First, the spatially uniform state must be stable to small perturbations, that is all $\lambda(k^2)$ in (14.22) have $\mathrm{Re}\,\lambda(k^2 = 0) < 0$, and second, only patterns of a certain spatial extent, that is patterns within a definite range of wavelengths k, can begin to grow, with $\mathrm{Re}\,\lambda(k^2 \neq 0) > 0$. These conditions are encapsulated in the dispersion relation in either the (λ, k^2) or (λ, ω^2) forms such as in Fig. 14.4 (b) and Fig. 14.5 (a). The latter, for example, also says that if the spatial pattern of the disturbances have k^2 large, that is, very small wavelength disturbances, the steady state is again linearly stable. A dispersion relation therefore immediately gives the initial rate of growth or decay of patterns of various sizes. Dispersion relations are obtained from the general evolution equations of the pattern formation mechanism. A

general and non-technical biologically oriented discussion of pattern formation models is given by Oster and Murray (1989).

Since the solutions to the linear eigenfunction equations such as (14.36) are simply sines and cosines, the 'size' of various spatial patterns is measured by the wavelength of the trigonometric functions; for example $\cos(n\pi x/p)$ has a wavelength $\omega = 2p/n$. So, the search for growing spatial patterns comes down to seeing how many sine or cosine waves can 'fit' into a domain of a given size. The two-dimensional situation is similar, but with more flexibility as to how they fit together.

A very important use of the dispersion relation is that it shows immediately whether patterns can grow, and if so, what the size of the patterns are. The curves in Fig. 14.4 (b) and Fig. 14.5 (a) are the prototype – no frills or 'vanilla' – dispersion relation for generating spatial patterns. We shall see later that other forms are possible and imply different pattern formation phenomena. However, these are less common and little is known at the present time about the patterns which evolve from them. The mechanochemical models discussed in detail in Chapter 17 can in fact generate a surprisingly rich spectrum of dispersion relations (see Murray and Oster 1984) most of which cannot be generated by two or three-species reaction diffusion models.

The prototype dispersion relation has the two essential characteristics mentioned above: (i) the spatially featureless state ($k = 0$, $\omega = \infty$) is stable: that is, the growth rate of very large wavelength waves is negative, and (ii) there is a small band, or window, of wavelengths which can grow (that is, a finite band of unstable 'modes', $\cos(n\pi x/L)$, for a finite number of integers n). Of these growing modes, one grows fastest; the one closest to the peak of the dispersion curve. This mode, k_m say, is the solution of

$$\frac{\partial \lambda}{\partial k^2} = 0 \quad \Rightarrow \quad \max[\mathrm{Re}\,\lambda] = \mathrm{Re}\,\lambda(k_m^2)\,.$$

Strictly k_m may not be an allowable mode in a finite domain situation. In this case it is the possible mode closest to the analytically determined k_m.

Thus the dispersion curve shows that while the spatially homogeneous state is stable, the system will amplify patterns of a particular spatial extent, should they be excited by random fluctuations, which are always present in a biological system, or by cues from earlier patterns in development. Generally, one of the model parameters is 'tuned' until the dispersion curve achieves the qualitative shape shown. For example, in Fig. 14.4 (b) if the diffusion ratio d is less than the critical d_c, $\mathrm{Re}\,\lambda < 0$ for all k^2. As d increases, the curve rises until $d = d_c$ after which it pushes its nose above the axis at some wavenumber k_c, that is wavelength $\omega_c = 2\pi/k_c$, whereupon a cosine wave of that wavelength can start to grow, assuming it is an allowable eigenfunction. This critical wavenumber is given by (14.28) and, with $d = d_c$ from (14.27), we thus have

$$\omega_c = \frac{2\pi}{k_c} = 2\pi\left\{\frac{d_c}{\gamma^2(f_u g_v - f_v g_u)}\right\}^{1/4}. \tag{14.54}$$

With the illustrative example (14.32) there are 4 dimensionless parameters: a and b, the kinetics parameters, d, the ratio of diffusion coefficients and γ, the scale parameter. We concentrated on how the dispersion relation varied with d and showed how a bifurcation value d_c existed when the homogeneous steady state became unstable, with the pattern 'size' determined by k_c or ω_c given by the last equation. It is very useful to know the parameter space, involving all the parameters, wherein pattern forms and how we move into this pattern forming domain by varying whatever parameter we choose, or indeed when we vary more than one parameter. Clearly the more parameters there are the more complicated is this corresponding parameter or Turing space. Let us now determine the parameter space for the model (14.32) by extending the parametric method we described in Chapter 6, Section 6.4 for determining the space in which oscillatory solutions were possible. The technique was developed and applied to several reaction diffusion models by Murray (1982).

The conditions on the parameters a, b and d for the mechanism (14.32) to generate spatial patterns, if the domain is sufficiently large, are given by (14.35) with γ coming into the picture via the possible unstable modes determined by (14.38). Even though the inequalities (14.35) are probably the simplest realistic set we could have in any reaction diffusion mechanism they are still algebraically quite messy to deal with. With other than extremely simple kinetics it is not possible to carry out a similar analysis analytically. So let us start with the representation of the steady state used in Section 6.4, namely (6.24), with u_0 as the nonnegative parametric variable; that is v_0 and b are given in terms of a and u_0 from (6.24), or (14.33) above, as

$$v_0 = \frac{u_0 - a}{u_0^2}, \quad b = u_0 - a\,. \tag{14.55}$$

The inequalities (14.35), which define the conditions on the parameters for spatial patterns to grow, involve, on using the last expressions,

$$\begin{aligned} f_u &= -1 + 2u_0v_0 = 1 - \frac{2a}{u_0}, \quad f_v = u_0^2\,, \\ g_u &= -2u_0v_0 = -\frac{2(u_0 - a)}{u_0}, \quad g_v = -u_0^2\,. \end{aligned} \tag{14.56}$$

We now express the conditions for diffusion-driven instability given by (14.31) as inequalities in terms of the parameter u_0: these define boundary curves for domains in parameter space. With the first,

$$\begin{aligned} & f_u + g_v < 0 \quad \Rightarrow \quad 1 - \frac{2a}{u_0} - u_0^2 < 0 \\ & \Rightarrow \quad a > \frac{u_0(1 - u_0^2)}{2}, \quad b < u_0 - a = \frac{u_0(1 + u_0^2)}{2}\,, \\ & \Rightarrow \quad b = \frac{u_0(1 + u_0^2)}{2} \end{aligned} \tag{14.57}$$

as the boundary curve where, since we are interested in the boundary curve, the $b = u_0 - a$ comes from the steady state definition (14.55) and where we replace a by its expression from the inequality involving only u_0 and a. These define a domain parametrically in (a, b) space as we let u_0 take all positive values; if the inequality is replaced by an equality sign, (14.57) define the boundary curve parametrically. We now do this with each of the conditions in (14.31).

The second condition of (14.31), using (14.56), requires

$$f_u g_v - f_v g_u > 0 \quad \Rightarrow \quad u_0^2 > 0\,, \tag{14.58}$$

which is automatically satisfied. The third condition, requires

$$\begin{aligned} & df_u + g_v > 0 \\ \Rightarrow \quad & a < \frac{u_0(d-u_0^2)}{2d}, \quad b = u_0 - a = \frac{u_0(d+u_0^2)}{2d}\,, \\ \Rightarrow \quad & b = \frac{u_0(d+u_0^2)}{2d} \end{aligned} \tag{14.59}$$

as the boundary curve.

The fourth condition in (14.31) is a little more complicated. Here

$$\begin{aligned} & (df_u + g_v)^2 - 4d(f_u g_v - f_v g_u) > 0 \\ \Rightarrow \quad & [u_0(d-u_0^2) - 2da]^2 - 4du_0^4 > 0 \\ \Rightarrow \quad & 4a^2d^2 - 4adu_0(d-u_0^2) + [u_0^2(d-u_0^2)^2 - 4u_0^4 d] > 0 \end{aligned}$$

which, on factorizing the left hand side, implies

$$a < u_0\frac{1 - \frac{2u_0}{\sqrt{d}} - \frac{u_0^2}{d}}{2} \quad \text{or} \quad a > u_0\frac{1 + \frac{2u_0}{\sqrt{d}} - \frac{u_0^2}{d}}{2}\,.$$

Thus this inequality results in *two* boundary curves, namely

$$\begin{aligned} & a = u_0\frac{1 - \frac{2u_0}{\sqrt{d}} - \frac{u_0^2}{d}}{2}, \quad b = u_0 - a = u_0\frac{1 + \frac{2u_0}{\sqrt{d}} + \frac{u_0^2}{d}}{2}\,, \\ & a = u_0\frac{1 + \frac{2u_0}{\sqrt{d}} - \frac{u_0^2}{d}}{2}, \quad b = u_0 - a = u_0\frac{1 - \frac{2u_0}{\sqrt{d}} + \frac{u_0^2}{d}}{2}\,. \end{aligned} \tag{14.60}$$

The curves, and the enclosed domains, defined parametrically by (14.57)-(14.60), define the parameter space or *Turing space* (see Murray 1982), where the steady state can be diffusionally driven unstable and hence create spatial patterns. As we noted in Section 14.4 the first and third conditions in (14.35) require f_u and g_v to have opposite signs which require $b > a$ and hence $d > 1$.

It is now a straightforward plotting exercise to obtain the curves defined by (14.57)–(14.60): we simply let u_0 take on a range of positive values and calculate

the corresponding a and b for a given d. In general, with inequalities (14.57)–(14.60), five curves are involved in defining the boundaries. Here, as is often the case, several are redundant in that they are covered by one of the others. For example, in the first of (14.60),

$$a < u_0\frac{1 - \frac{2u_0}{\sqrt{d}} - \frac{u_0^2}{d}}{2} < u_0\frac{1 - \frac{u_0^2}{d}}{2}\,,$$

since we are considering $u_0 > 0$, so (14.59) is automatically satisfied if we satisfy the first condition in (14.60). Also, since $d > 1$,

$$u_0\frac{1 - \frac{u_0^2}{d}}{2} > u_0\frac{1 - u_0^2}{2}$$

so the curve defined by (14.57) lies below the curve defined by (14.59): the former is a lower limiting boundary curve, so a suitable domain is defined if we use the first of (14.60). Furthermore, since

$$u_0\frac{1 - \frac{u_0^2}{d}}{2} < u_0\frac{1 + \frac{2u_0}{\sqrt{d}} - \frac{u_0^2}{d}}{2}$$

there can be no domain satisfying (14.59) and the second curve in (14.60).

Finally, therefore, for this mechanism we need only two parametric curves, namely those defined by (14.57) and the first of (14.60), and the Turing space is determined by

$$\begin{aligned} & a > u_0\frac{1 - u_0^2}{2}, \quad b = u_0\frac{1 + u_0^2}{2}\,, \\ & a < u_0\frac{1 - \frac{2u_0}{\sqrt{d}} - \frac{u_0^2}{d}}{2}, \quad b = u_0\frac{1 + \frac{2u_0}{\sqrt{d}} + \frac{u_0^2}{d}}{2}\,. \end{aligned} \tag{14.61}$$

We know that when $d = 1$ there is no Turing space, that is there is no domain where spatial patterns can be generated. The curves defined by (14.61) with $d = 1$ contradict each other and hence no Turing space exists. Now let d take on values greater than 1. For a critical d, d_c say, a Turing space starts to grow for $d > d_c$. Specifically $d = d_c = 3 + 2\sqrt{2}$, calculated from (14.61) by determining the d such that both curves give $a = 0$ at $b = 1$ and at this value the two inequalities are no longer contradictory. The space is defined, in fact, by two surfaces in (a, b, d) space. Fig. 14.9 shows the cross-sectional regions in (a, b) parameter space where the mechanism (14.32) can generate spatial patterns.

Even if a and b, for a given $d > 1$, lie within the Turing space this does not guarantee that the mechanism will generate spatial patterns, because scale and geometry play a major role. Depending on the size of γ and the actual spatial domain in which the mechanism operates, the unstable eigenfunctions, or modes,

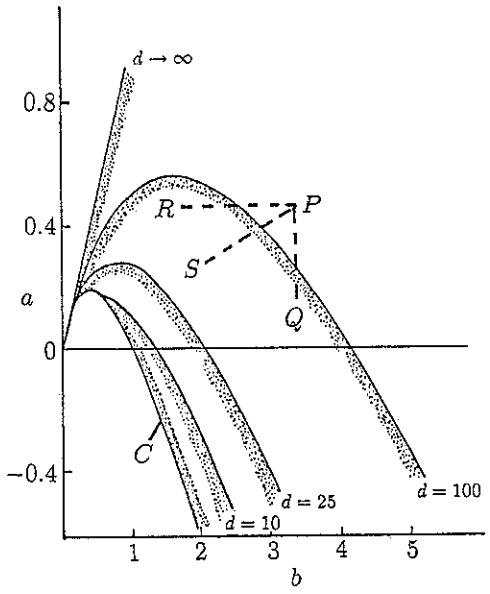

Fig. 14.9. Turing space for (14.32); that is the parameter space where spatial patterns can be generated by the reaction diffusion mechanism (14.32). For example, if $d = 25$ any values for a and b lying within the domain bounded by the curves marked C (that is $d = 1$) and $d = 25$ will result in diffusion driven instability. Spatial pattern will evolve if the domain (γ) is sufficiently large for allowable k^2, defined by (14.38) and (14.43).

may not be allowable solutions. It is here that the detailed form of the dispersion relation comes in again. To be specific let us consider the one-dimensional finite domain problem defined by (14.36). The eigenvalues, that is the wavenumbers, $k = n\pi/p$, $n = \pm 1, \pm 2 \ldots$ are *discrete*. So, referring to Fig. 14.4 (b), unless the dispersion relation includes in its range of unstable modes at least one of these discrete values no structure can develop. We must therefore superimpose on the Turing space in Fig. 14.9 another axis representing the scale parameter γ. If γ is included in the parameters of the Turing space it is not necessarily simply connected since, if the dispersion relation, as γ varies, does not include an allowable eigenfunction in its unstable modes, no pattern evolves. Let us consider this aspect and use of the dispersion relation in more detail.

The Turing space involves only dimensionless parameters which are appropriate groupings of the dimensional parameters of the model. The parameters a, b and d in the last figure are, from (14.6),

$$a = \frac{k_1}{k_2}\left(\frac{k_3}{k_2}\right)^{1/2}, \quad b = \frac{k_4}{k_2}\left(\frac{k_3}{k_2}\right)^{1/2}, \quad d = \frac{D_B}{D_A}.$$

Suppose, for example, $d = 100$ and a and b have values associated with P in Fig. 14.9, that is the mechanism is not in a pattern formation mode. There is no unique way to move into the pattern formation domain; we could decrease either a or b so that we arrive at Q or R respectively. In dimensional terms we can reduce a, for example, by appropriately changing k_1, k_2 or k_3 – or all of them. Varying other than k_1 will also affect b, so we have to keep track of b as well. If we only varied k_2 the path in the Turing space is qualitatively like that from P to

S. If d can vary, which means either of D_A or D_B can vary, we can envelope P in the pattern formation region by simply increasing d. Interpreting the results from a biological point of view, therefore, we see that it is the *orchestration of several effects which produce pattern*, not just one, since we can move into the pattern formation regime by varying one of several parameters. Clearly we can arrive at a specific point in the space by one of several paths. The concept of equivalent effects, via parameter variation, producing the same pattern is an important one in the interpretation and design of relevant experiments associated with any model. It is not a widely appreciated concept in biology. We shall discuss some important biological applications of the practical use of dimensionless groupings in subsequent chapters.

To recap briefly, the dispersion relation for the general reaction diffusion system (14.10) is given by the root $\lambda(k^2)$ of (14.23) with the larger real part. The key to the existence of unstable spatial modes is whether or not the function

$$h(k^2) = dk^4 - \gamma(df_u + g_v)k^2 + \gamma^2(f_u g_v - f_v g_u) \tag{14.62}$$

is negative for a range of $k^2 \neq 0$: see Fig. 14.4 (a). Remember that the f and g derivatives are evaluated at the steady state (u_0, v_0) where $f(u_0, v_0) = g(u_0, v_0) = 0$, so $h(k^2)$ is a quadratic in k^2 whose coefficients are functions only of the parameters of the kinetics, d the diffusion coefficient ratio and the scale parameter γ. The minimum, $h_{\min}$, at $k = k_m$ corresponds to the λ with the maximum $\mathrm{Re}\,\lambda$ and hence the mode with the largest growth factor $\exp[\lambda(k_m^2)t]$. From (14.25), or simply from the last equation, $h_{\min}$ is given by

$$\begin{aligned} h_{\min} &= h(k_m^2) = -\gamma^2 \frac{df_u^2 + \frac{g_v^2}{d} - 2(f_u g_v - 2f_v g_u)}{4}, \\ k_m^2 &= \gamma \frac{df_u + g_v}{2d}. \end{aligned} \tag{14.63}$$

The bifurcation between spatially stable and unstable modes is when $h_{\min} = 0$. When this holds there is a critical wave number k_c which, from (14.28) or again simply derived from (14.62), is when the parameters are such that

$$(df_u + g_v)^2 = 4d(f_u g_v - f_v g_u) \quad \Rightarrow \quad k_c^2 = \gamma \frac{df_u + g_v}{2d}. \tag{14.64}$$

As the parameters move around the Turing space we can achieve the required equality, the first of the equations in (14.64), by letting one or other of the parameters pass through its bifurcation values, all other parameters being kept fixed. In the last section, and in Fig. 14.4 (b) for example, we chose d as the parameter to vary and for given a and b we evaluated the bifurcation value d_c. In this situation, just at bifurcation, that is, when $h_{\min}(k_c^2) = 0$, a single spatial pattern with wavenumber k_c is driven unstable, or excited, for $d = d_c + \varepsilon$, where $0 < \varepsilon \ll 1$. This critical wavenumber from (14.64) is proportional to $\sqrt{\gamma}$ and so

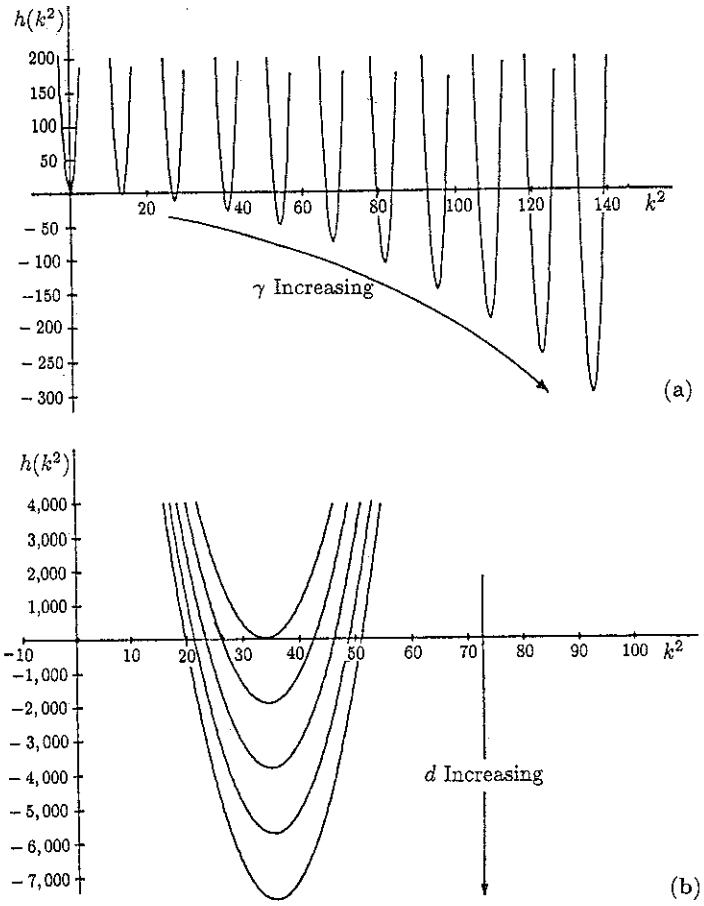

Fig. 14.10a,b. (a) Isolation of unstable modes (that is $h(k^2) < 0$ in (14.23)) by setting the diffusion ratio $d = d_c + \varepsilon$, $0 < \varepsilon \ll 1$ and varying the scale γ for the Thomas (1975) kinetics (14.8) with $a = 150$, $b = 100$, $\alpha = 1.5$, $\rho = 13$, $K = 0.05$, $d = 27.03$: the critical $d_c = 27.02$. (b) The effect of increasing d with all other parameters fixed as in (a). As $d \to \infty$ the range of unstable modes is bounded by $k^2 = 0$ and $k^2 = \gamma f_u$.

we can vary which spatial pattern is initiated by varying γ. This is called *mode selection* and is crucial in applications as we shall see later.

In the case of finite domains we can isolate a specific mode to be excited, or driven unstable, by choosing the width of the band of unstable wavenumbers to be narrow and centred round the desired mode. Let us take the parameters in the kinetics to be fixed and let $d = d_c + \varepsilon$, $0 < \varepsilon \ll 1$ we then get from (14.64) the appropriate γ for a specified k as

$$\gamma \approx \frac{2d_c k^2}{d_c f_u + g_v}\,, \tag{14.65}$$

where the kinetics parameters at bifurcation, sometimes called the *marginal kinetics state*, satisfy the first of (14.64). So, by varying γ we can isolate whatever mode we wish to be excited. Fig. 14.10 (a) shows a typical situation. Arcuri and Murray (1986) have carried out an extensive Turing space analysis for the Thomas (1975) mechanism in such a case. Note in Fig. 14.10 (a) that as γ increases $h_{\min}$ becomes more negative, as is indicated by (14.63).

Suppose now we keep γ and the kinetics parameters fixed, and let d increase from its bifurcation value d_c. From (14.63) $h_{\min} \sim -(\gamma f_u)^2 d/4$ for d large and so $\lambda \to \infty$ with d. The width of the band of unstable modes has wavenumbers bounded by the zeros k_1 and k_2 of $h(k^2)$ in (14.62). These are given by (14.29), or immediately from (14.62) as

$$\begin{aligned} k_1^2 &= \gamma \frac{(df_u + g_v) - \{(df_u + g_v)^2 - 4d(f_u g_v - f_v g_u)\}^{1/2}}{2d}\,, \\ k_2^2 &= \gamma \frac{(df_u + g_v) + \{(df_u + g_v)^2 - 4d(f_u g_v - f_v g_u)\}^{1/2}}{2d}\,, \end{aligned} \tag{14.66}$$

from which we get

$$k_1^2 \sim 0, \quad k_2^2 \sim \gamma f_u \quad \text{as} \quad d \to \infty\,. \tag{14.67}$$

So, for a fixed scale there is an upper limit for the excited mode wavenumber and hence a lower limit for the possible wavelengths of the spatial patterns. Fig. 14.10 (b) illustrates a typical case for the Thomas (1975) system given by (14.8).

With all kinetics parameters fixed, each parameter pair (d, γ) defines a unique parabola $h(k^2)$ in (14.62), which in turn specifies a set of unstable modes. We can thus consider the (d, γ) plane to be divided into regions where specific modes or a group of modes are diffusively unstable. When there are several unstable modes, because of the form of the dispersion relation, such as in Fig. 14.4 (b), there is clearly a mode with the largest growth rate since there is a maximum $\mathrm{Re}\,\lambda$ for some k_m^2 say. From (14.23), the positive eigenvalue $\lambda_+(k^2)$ is given by

$$2\lambda_+(k^2) = \gamma(f_u + g_v) - k^2(1 + d) + \{[\gamma(f_u + g_v) - k^2(1 + d)]^2 - 4h(k^2)\}^{1/2}$$

which has a maximum for the wavenumber k_m given by

$$k^2 = k_m^2 = \frac{\gamma}{d - 1}\left\{(d + 1)\left[-\frac{f_v g_u}{d}\right]^{1/2} - f_u + g_v\right\}\,. \tag{14.68}$$

As we have noted the prediction is that the fastest growing k_m-mode will be that which dominates and hence will be the mode which evolves into the steady state nonlinear pattern. This is only a reasonable prediction for the lower modes. The probable reason is that with the higher modes the interaction caused by the nonlinearities is more complex than when only the simpler modes are linearly

unstable. Thus using (14.68) we can map the regions in (d, γ) space where a specific mode, and hence pattern, will evolve: see Arcuri and Murray (1986). Fig. 14.11 (a), (b) show the mappings for the Thomas (1975) system in one space dimension calculated from the linear theory and the full nonlinear system, while Fig. 14.11 (c) shows the corresponding spatial morphogen patterns indicated by Fig. 14.11 (b).

An important use of such parameter spaces is the measure of the robustness of the mechanism under consideration. With Fig. 14.11 (b), for example, suppose the biological conditions result in a (d, γ) parameter pair giving P, say, in the region which evolves to the 4-mode. A key property of any model is how sensitive it is to the inevitable random perturbations which exist in the real world. From Fig. 14.11 (b) we see what leeway there is if a 4-mode pattern is required in the developmental sequence. This (d, γ) space is but one of the relevant spaces to consider, of course, since any mechanism involves other parameters. So, in assessing robustness, or model sensitivity, we must also take into account the size and shape of the Turing space which involves all of the kinetics parameters. Probably (d, γ) spaces will not be too different qualitatively from one reaction diffusion system to another. What certainly is different, however, is the size and shape of the Turing space, and it is this space which provides another useful criterion for comparing relevant robustness of models. Murray (1982) studied this specific problem and compared various specific reaction diffusion mechanisms with this in mind. He came to certain conclusions as to the more robust mechanisms – both the Thomas (1975) and Schnakenberg (1979) systems, given respectively by (14.7) and (14.8), have relatively large Turing spaces, whereas that of the activator-inhibitor model of Gierer and Meinhardt (1972), given by (14.9) is quite small and implies a considerable sensitivity of pattern to small parameter variation. In the next chapter on specific pattern formation problems in biology we touch on other important aspects of model relevance which are implied by the form of the dispersion relation and the nondimensionalisation used.

The parameter spaces designating areas for specific patterns were all obtained with initial conditions taken to be random perturbations about the uniform steady state. Even in the low modes the polarity can be definitively influenced by biased initial conditions. We can, for example, create a single hump pattern with a single maximum in the centre of the domain or with a single minimum in the centre: see Fig. 14.6 (b). So even though specific modes can be isolated, initial conditions can strongly influence the polarity. When several of the modes are excitable, and one is naturally dominant from the dispersion relation, we can still influence the ultimate pattern by appropriate initial conditions. If the initial conditions include a mode within the unstable band and whose amplitude is sufficiently large, then this mode can persist through the nonlinear region so as to dominate the other unstable modes and the final pattern qualitatively often has roughly that wavelength. We discuss this in more detail in the next section. These facts also have highly relevant implications for biological applications.

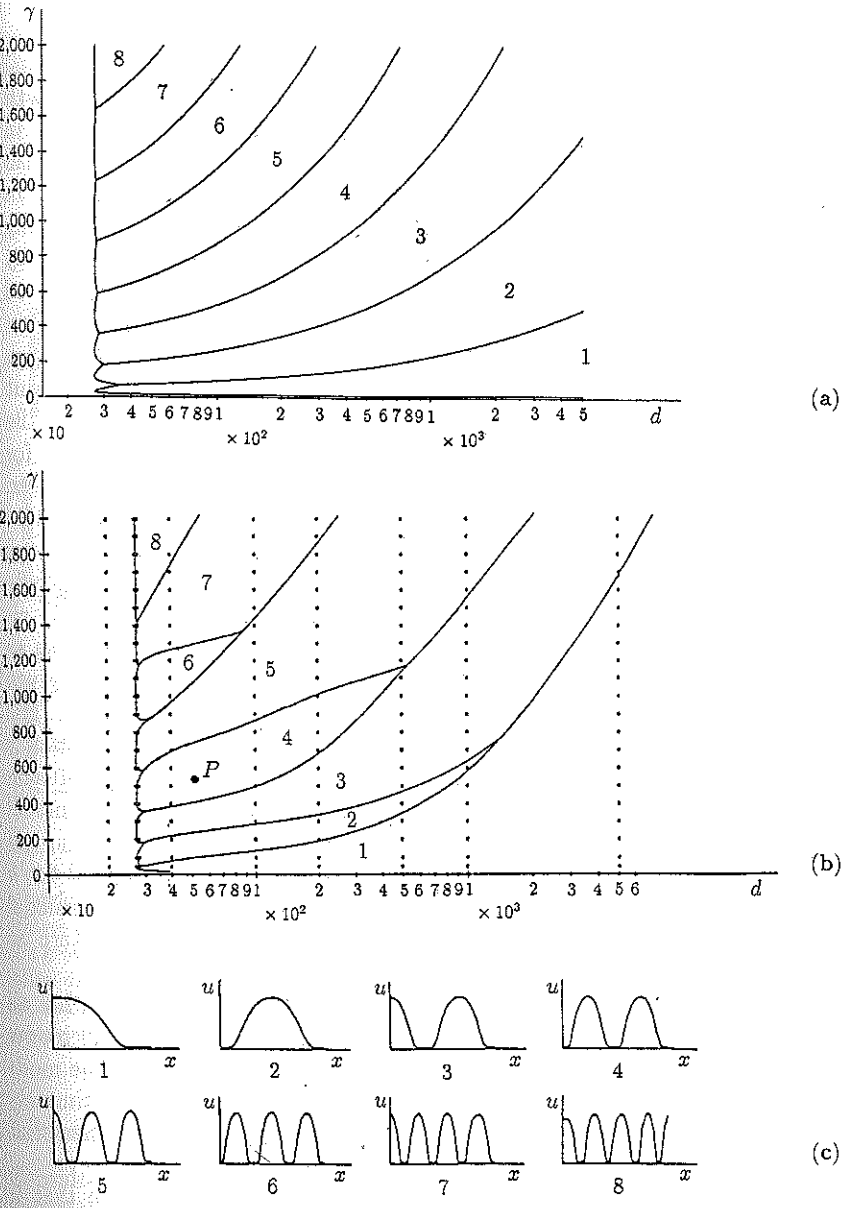

Fig. 14.11a-c. (a) Predicted solution space, based on linear theory, showing the regions with the fastest growing modes for the Thomas (1975) system (14.8) with parameter values as in Fig. 14.10 and zero flux boundary conditions. (b) A typical space as evaluated from the numerical simulation of the full nonlinear Thomas system (14.8) with the same parameter values and zero flux boundary conditions as in (a). Each (γ, d) point marked with a period represents a specific simulation of the full nonlinear system. (c) The corresponding spatial morphogen concentration patterns obtained with parameters d and γ in the regions indicated in (b). Spatial patterns can be visualised by setting a threshold u^* and shading for $u > u^*$. The first two morphogen distributions, for example, correspond to the first two patterns in Fig. 14.7. (From Arcuri and Murray 1986)

14.6 Mode Selection and the Dispersion Relation

Consider a typical 'vanilla' or simplest dispersion relation giving the growth factor λ as a function of the wavenumber or wavelength ω such as shown in Fig. 14.4 (b) where a band of wavenumbers is linearly unstable. Let us also suppose the domain is finite so that the spectrum of eigenvalues is discrete. In the last section we saw how geometry and scale played key roles in determining the particular pattern predicted from linear theory, and this was borne out by numerical simulation of the nonlinear system: see also the results presented in the next chapter. We pointed out that initial conditions can play a role in determining, for example, the polarity of a pattern or whether a specific pattern will emerge. If the initial conditions consist of small random perturbations about the uniform steady state then the likely pattern to evolve is that with the largest linear growth. In many developmental problems, however, the trigger for pattern initiation is scale – there are several examples in the following chapter. In other developmental situations a perturbation from the uniform steady state is initiated at one end of the spatial domain and the spatial pattern develops from there, eventually spreading throughout the whole domain. The specific pattern that evolves for a given mechanism therefore can depend critically on how the instability is initiated. In this section we investigate this further so as to suggest what patterns will evolve from which initial conditions, for given dispersion relations, as key parameters pass through bifurcation values. The problem of which pattern will evolve, namely mode selection, is a constantly recurring one. The following discussion, although motivated by reaction diffusion pattern generators, is quite general and applies to any pattern formation model which produces a similar type of dispersion relation.

Consider a basic dispersion relation $\lambda(\omega^2)$ where the wavelength $\omega = 2\pi/k$ with k the wavenumber, such as in Fig. 14.12 (a). Now take a one-dimensional domain and consider in turn the three possible ways of initiating pattern as shown in Fig. 14.12 (b), (c), (d).

Consider first the case in Fig. 14.12 (b). Here the initial perturbation has all modes present in its expansion in terms of the eigenfunctions and so all modes in the unstable band of wavelengths in Fig. 14.12 (a) are stimulated. The mode with the maximum λ, ω_2, is the one with the fastest growth and it ultimately dominates. The steady state inhomogeneous pattern that persists is then that with wavelength ω_2.

In Fig. 14.12 (c) we envisage the domain to be growing at a rate that is slow compared with the time to generate spatial pattern. For small $L(t)$ the domain is such that it cannot contain any wave with wavelengths in the unstable band. When it reaches L_c, the critical domain size for pattern, it can sustain the smallest wavelength pattern, namely that with wavelength ω_1. In the time it takes $L(t)$ to grow sufficiently to allow growth of the next wavenumber, that with wavelength ω_1 is sufficiently established to dominate the nonlinear stage. So the final pattern that emerges is that with the base wavelength ω_1.

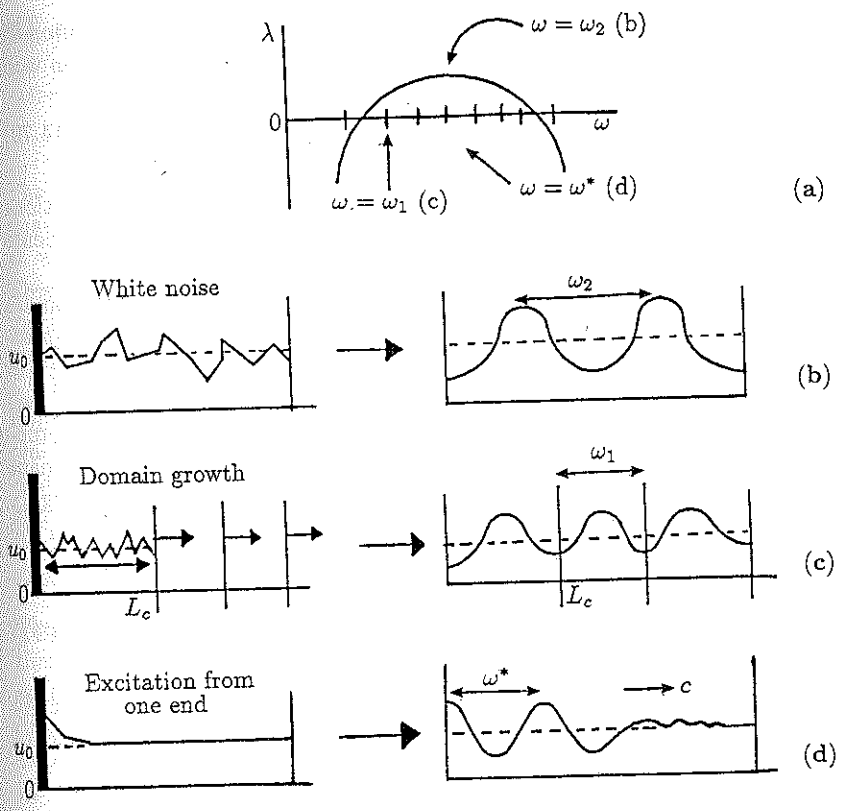

Fig. 14.12a-d. (a) Typical basic, or 'vanilla', dispersion relation giving the growth coefficient λ as a function of the wavelength ω of the spatial pattern. (b) Here the initial disturbance is a random perturbation (white noise) about the uniform steady state u_0. The pattern which evolves corresponds to ω_2 in (a), the mode with the largest growth rate. (c) Pattern evolution in a growing domain. The first unstable mode to be excited, ω_1, remains dominant. (d) Here the initial disturbance is at one end and it lays down a pattern as the disturbance moves through the domain. The pattern which evolves has a wavelength ω^* somewhere within the band of unstable wavelengths.

Travelling Wave Initiation of Pattern

Consider the situation, as in Fig. 14.12 (d), where the pattern is initiated at one end of the domain. We expect the final pattern to have a wavelength somewhere within the unstable band predicted by the dispersion relation. To see how to calculate the wavenumber in general let us start with an infinite one-dimensional domain and a general linear system

$$\mathcal{J}\mathbf{w} = 0, \quad \mathbf{w}(x,t) \propto \exp(ikx + \lambda t) \quad \Rightarrow \quad \lambda = \lambda(k)\,, \tag{14.69}$$

where $\mathcal{J}$ is a linear operator such as associated with the linear form of reaction

or in the last figure with ω replaced by k; in other words the classic form. The general solution $\mathbf{w}$ of the linear system in (14.69) is

$$\mathbf{w}(x,t) = \int \mathbf{A}(k) \exp\left[ikx + \lambda(k)t\right] dk \,, \tag{14.70}$$

where the $\mathbf{A}(k)$ are determined by a Fourier transform of the initial conditions $\mathbf{w}(x,0)$. Since we are concerned with the final structure and not the transients we do not need to evaluate $\mathbf{A}(k)$ here.

Suppose the initial conditions $\mathbf{w}(x,0)$ are confined to a small finite domain around $x = 0$ and the pattern propagates out from this region. We are interested in the wave-like generation of pattern as shown in the second figure in Fig. 14.12 (d). This means that we should look at the form of the solution well away from the origin. In other words, we should focus our attention on the asymptotic form of the solution for x and t large but such that x/t is $O(1)$, which means we move with a velocity $c = x/t$ and so are in the vicinity of the 'front' – roughly where the arrow is in the second figure in Fig. 14.12 (d). We write (14.70) in the form

$$\mathbf{w}(x,t) = \int \mathbf{A}(k) \exp\left[\sigma(k)t\right] dk, \quad \sigma(k) = ikc + \lambda(k), \quad c = \frac{x}{t} \,. \tag{14.71}$$

The asymptotic evaluation of this integral for $t \to \infty$ is given by analytically continuing the integrand into the complex k-plane and using the method of steepest descents (see Murray's (1984) book, Chapter 3) which gives

$$\mathbf{w}(x,t) \sim \mathbf{J}(k_0) \left[\frac{2\pi}{t|\sigma''(k_0)|}\right]^{1/2} \exp\left\{t[ik_0c + \lambda(k_0)]\right\}$$

where $\mathbf{J}$ is a constant and k_0 (now complex) is given by

$$\sigma'(k_0) = ic + \lambda'(k_0) = 0 \,. \tag{14.72}$$

The asymptotic form of the solution is thus

$$\mathbf{w}(x,t) \sim \mathbf{K} t^{-1/2} \exp\left\{t[ick_0 + \lambda(k_0)]\right\} \tag{14.73}$$

where $\mathbf{K}$ is a constant.

For large t the wave 'front' is roughly the point between the pattern forming tail and the leading edge which initiates the disturbances, that is, where $\mathbf{w}$ neither grows nor decays. This is thus the point where

$$\mathrm{Re}\left[ick_0 + \lambda(k_0)\right] \approx 0 \,. \tag{14.74}$$

At the 'front' the wavenumber is $\mathrm{Re}\, k_0$ and the solution frequency of oscillation ω is

$$\omega = \mathrm{Im}\left[ick_0 + \lambda(k_0)\right] \,.$$

Denote by k^* the wavenumber of the pattern laid down behind the 'front'. We now assume there is conservation of nodes across the 'front' which implies

$$k^*c = \omega = \mathrm{Im}\left[ick_0 + \lambda(k_0)\right] \,. \tag{14.75}$$

The three equations (14.72), (14.74) and (14.75) now determine k_0 and the quantities we are interested in, namely c and k^*, are respectively the speed at which the pattern is laid down and the steady state pattern wavenumber. This technique has been used by Dee and Langer (1983) for a reaction diffusion mechanism. They simulate the dynamics of the pattern generation for a specific system.

Becker and Field (1985) obtained spatial patterns from a numerical simulation of the Field-Noyes model, with diffusion, for the Belousov-Zhabotinskii reaction discussed in Chapter 7. They also found such patterns experimentally. Stationary spatial patterns in the BZ reaction were also obtained numerically and experimentally by Varek et al. (1979).

Dynamics of Pattern Formation in Growing Domains

The time evolution of patterns in growing domains can be quite complex, particularly if the domain growth is comparable with the generation time of the spatial pattern and there are two or more space dimensions. The form of the dispersion relation as the scale γ increases can have highly pertinent biological implications as we shall see in Chapter 17 when we consider cartilage formation in the developing limb. Here we introduce the phenomenon and discuss some of the implications of two specific classes of dispersion relation behaviour as γ increases.

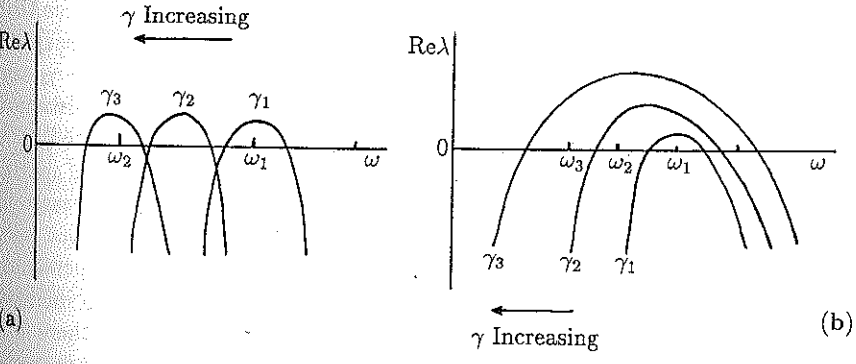

Fig. 14.13a,b. (a) As the scale γ increases from γ_1 to γ_3 the dispersion relation isolates specific modes interpersed with gaps during which no pattern can form. (b) Here as γ increases the number of unstable modes increases: the mode with maximum growth varies with γ. Unstable modes exist for all $\gamma \geq \gamma_1$.

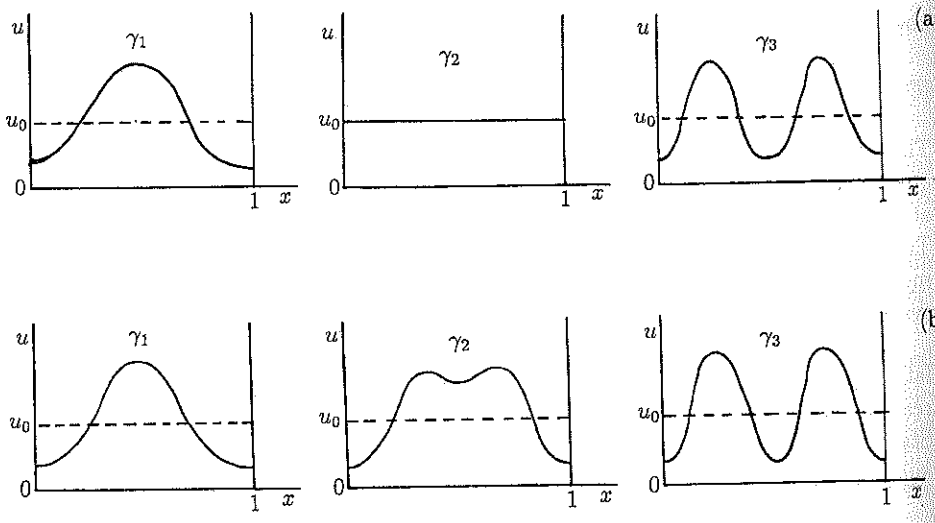

Fig. 14.14a,b. (a) Development of spatial patterns with a dispersion relation dependence on scale, via γ, as shown in Fig. 14.13 (a). (b) Sequential development of pattern as γ varies according to the dispersion relation in Fig. 14.13 (b).

In Fig. 14.6 (a) we saw that as the scale γ increased the dispersion curve was moved along the axis where it successively excited modes with smaller wavelengths. Fig. 14.13 (a) is a repeat example of this behaviour. Fig. 14.13 (b) is another possible behaviour of a dispersion relation as the scale γ increases. They imply different pattern generation scenarios for growing domains.

Consider first the situation in Fig. 14.13 (a). Here for $\gamma = \gamma_1$ the mode with wavelength ω_1 is excited and starts to grow. As the domain increases we see that for $\gamma = \gamma_2$ no mode lies within the unstable band and so the pattern decays to the spatially uniform steady state. With further increase in scale, to $\gamma = \gamma_3$ say, we see that a pattern with wavelength ω_2 is created. So the pattern formation is effectively a discrete process with successively more structure created as γ increases but with each increase in structure interspersed with a regime of spatial homogeneity. Fig. 14.14 (a) illustrates the sequence of events as γ increases in the way we have just described.

Consider now the behaviour implied by the dispersion relation dependence on scale implied by Fig. 14.13 (b). Here the effect of scale is simply to increase the band of unstable modes. The dominant mode changes with γ so there is a continuous evolution from one mode, dominant for $\gamma = \gamma_1$ say, to another mode as it becomes dominant for $\gamma = \gamma_3$ say. This dynamic development of pattern is illustrated Fig. 14.14 (b).

When comparing different models with experiment it is not always possible to choose a given time as regards pattern generation to carry out the experiments. When it is possible, then perhaps similarity of pattern is a sufficient first step in

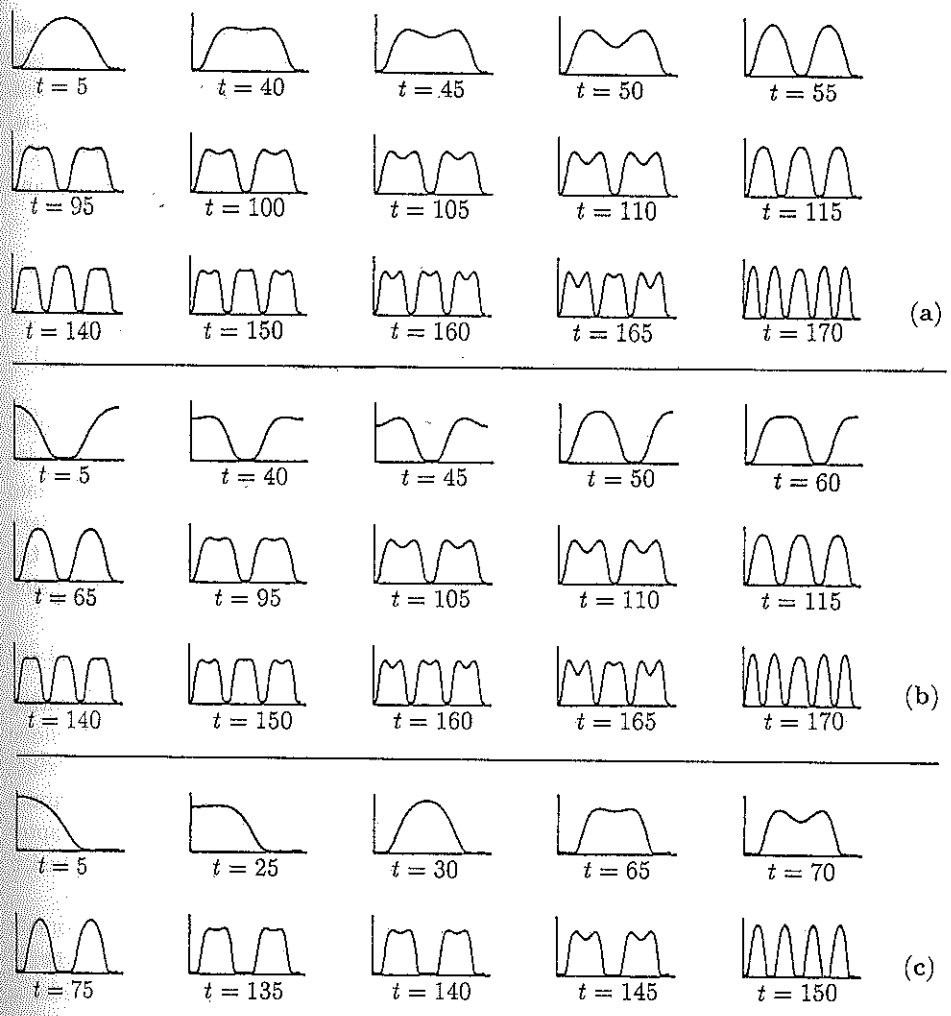

Fig. 14.15a-c. Sequence of one-dimensional spatial patterns numerically simulated with the mechanism (14.10) with kinetics (14.8). Zero flux boundary conditions were used and the growth in scale is $\gamma(t) = s + 0.1t^2$ with s fixed, which simulates a linear rate of growth since $\gamma \propto (\text{length})^2$. Parameter values for the kinetics are as in Fig. 14.10 (a) except for d. (a) and (b) have $d = 30$ ($d_c \approx 27$), $s = 100$ and two different sets of initial random perturbations. Note how the two sets of patterns converge as time t increases. (c) has $d = 60$, $s = 50$. As d increases more modes are missed in the pattern sequence and there is a distinct tendency towards frequency doubling. (After Arcuri and Murray 1986)

comparison with theory. When it is not possible, the dynamic form of the pattern can be important and can be the key step in deciding which mechanism is the more appropriate. We shall recall these comments later in Chapter 17.

A computed example of dynamic pattern formation as the scale γ is increased is shown in Fig. 14.15.

In these simulations the mechanism's pattern generation time is smaller than a representative growth time since the sequence of patterns clearly form before breaking up to initiate the subsequent pattern. This is an example of a dispersion breaking up to initiate the subsequent pattern. This is an example of a dispersion relation behaviour like that in Fig. 14.13 (b); that is there is no regime of spatial homogeneity. The tendency to period doubling indicated by Fig. 14.15 (c) is interesting and as yet unexplored. Arcuri and Murray (1986) consider this and other aspects of pattern formation in growing domains.

14.7 Pattern Generation with Single Species Models: Spatial Heterogeneity with the Spruce Budworm Model

We saw above that if the domain size is not large enough, that is γ is too small, reaction diffusion models with zero flux boundary conditions cannot generate spatial patterns. Zero flux conditions imply that the reaction diffusion domain is isolated from the external environment. We now consider different boundary conditions which take into account the influence of the region exterior to the reaction diffusion domain. To be specific, consider the single reaction diffusion equation in the form

$$u_t = f(u) + D\nabla^2 u \,, \tag{14.76}$$

and think of the model in an ecological setting; that is, u denotes the population density of a species. Here $f(u)$ is the species' dynamics and so we shall assume $f(0) = 0$, $f'(0) \neq 0$, $f(u_i) = 0$ for $i = 1$ if there is only one (positive) steady state or $i = 1, 2, 3$ if there are three. Later we shall consider the population dynamics $f(u)$ to be those of the spruce budworm, which we studied in detail in Chapter 1, Section 1.2 and which has three steady states as in Fig. 1.4. The diffusion coefficient D is a measure of the dispersal efficiency of the relevant species.

We consider in the first instance the one-dimensional problem for a domain $x \in (0, L)$, the exterior of which is completely hostile to the species. This means that on the domain boundaries $u = 0$. The mathematical problem we consider is then

$$\begin{aligned} &u_t = f(u) + Du_{xx} \,, \\ &u(0,t) = 0 = u(L,t), \quad u(x,0) = u_0(x) \,, \\ &f(0) = 0, \quad f'(0) > 0, \quad f(u_2) = 0, \quad f'(u_2) > 0 \,, \\ &f(u_i) = 0, \quad f'(u_i) < 0, \quad i = 1, 3 \,, \end{aligned} \tag{14.77}$$

where u_0 is the initial population distribution. The question we want to answer is whether or not such a model can sustain spatial patterns.

In the spatially homogeneous situation $u = 0$ and $u = u_2$ are unstable and u_1 and u_3 are stable steady states. In the absence of diffusion the dynamics imply that u tends to one or other of the stable steady states and which it is depends on the initial conditions. In the spatial situation, therefore, we would expect $u(x,t)$ to try to grow from $u = 0$ except at the boundaries. Because $u_x \neq 0$ at the boundaries the effect of diffusion implies that there is a flux of u out of the

domain $(0, L)$. So for u small there are two competing effects, the growth from the dynamics and the loss from the boundaries. As a first step we examine the linear problem obtained by linearising about $u = 0$. The relevant formulation is, from (14.77),

$$\begin{aligned} &u_t = f'(0)u + Du_{xx} \,, \\ &u(0,t) = u(L,t) = 0, \quad u(x,0) = u_0(x) \,. \end{aligned} \tag{14.78}$$

We look for solutions in the form

$$u(x,t) = \sum_n a_n e^{\lambda t} \sin(n\pi x/L) \,,$$

which by inspection satisfy the boundary conditions at $x = 0, L$. Substitution of this into (14.78) and equating coefficients of $\sin(n\pi x/L)$ determines λ as $\lambda = [f'(0) - D(n\pi/L)^2]$ and so the solution is given by

$$u(x,t) = \sum_n a_n \exp\left\{\left[f'(0) - D\left(\frac{n\pi}{L}\right)^2\right] t\right\} \sin\frac{n\pi x}{L} \,, \tag{14.79}$$

where the a_n are determined by a Fourier series expansion of the initial conditions $u_0(x)$. We do not need a_n in this analysis. From (14.79) we see that the dominant mode in the expression for u is that with the largest λ, namely that with $n = 1$, since

$$\exp\left[f'(0) - D\left(\frac{n\pi}{L}\right)^2\right] t < \exp\left[f'(0) - D\left(\frac{\pi}{L}\right)^2\right] t, \quad \text{for all} \quad n \geq 2 \,.$$

So, if the dominant mode tends to zero as $t \to \infty$, so then do all the rest. We thus get as our condition for the linear stability of $u = 0$

$$f'(0) - D\left(\frac{\pi}{L}\right)^2 < 0 \quad \Rightarrow \quad L < L_c = \pi\left[\frac{D}{f'(0)}\right]^{1/2} \,. \tag{14.80}$$

In dimensional terms D has units $\mathrm{cm}^2\mathrm{s}^{-1}$ and $f'(0)$ units s^{-1} since it is the linear birth rate (for u small $f(u) \approx f'(0)u$) which together give L_c in centimetres. Thus if the domain size L is less than the critical size L_c, $u \to 0$ as $t \to \infty$ and no spatial structure evolves. The larger the diffusion coefficient the larger is the critical domain size; this is in keeping with the observation that as D increases so also does the flux out of the region.

The scenario for spatial structure in a growing domain is that as the domain grows and L just passes the bifurcation length L_c, $u = 0$ becomes unstable and the first mode

$$a_1 \exp\left[f'(0) - D\left(\frac{\pi}{L}\right)^2 t\right] \sin\frac{\pi x}{L}$$

starts to grow with time. Eventually the nonlinear effects come into play and $u(x,t)$ tends to a steady state spatially inhomogeneous solution $U(x)$, which, from (14.77), is determined by

$$DU'' + f(U) = 0, \quad U(0) = U(L) = 0\,, \tag{14.81}$$

where the prime denotes differentiation with respect to x. Because $f(U)$ is nonlinear we cannot, in general, get an explicit solution for U.

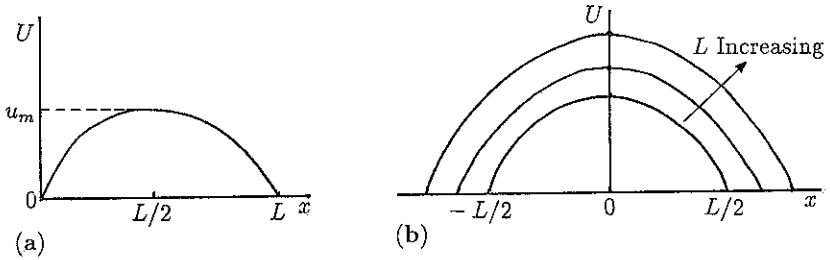

Fig. 14.16a,b. (a) Steady state pattern in the population u governed by (14.77) when the domain length $L > L_c$, the critical size for instability in the zero steady state. Note the symmetry about $L/2$. (b) Schematic steady state solution with the origin at the symmetry point where $u = u_m$ and $u_x = 0$.

From the spatial symmetry in (14.77) and (14.81) – setting $x \to -x$ leaves the equations unchanged – we expect the solutions to be symmetric in x about the mid-point $x = L/2$. Since $u = 0$ at the boundaries we assume the mid-point is the maximum, u_m say, where $U' = 0$: it is helpful now to refer to Fig. 14.16 (a). If we multiply (14.81) by U' and integrate with respect to x from 0 to L we get

$$\frac{1}{2}DU'^2 + F(U) = F(u_m), \quad F(U) = \int_0^U f(s)\,ds \tag{14.82}$$

since $U = u_m$ when $U' = 0$. It is convenient to change the origin to $L/2$ so that $U'(0) = 0$ and $U(0) = u_m$: that is set $x \to x - L/2$. Then

$$\left(\frac{D}{2}\right)^{1/2} \frac{dU}{dx} = [F(u_m) - F(U)]^{1/2}$$

which integrates to give

$$|x| = \left(\frac{D}{2}\right)^{1/2} \int_{U(x)}^{u_m} [F(u_m) - F(w)]^{-1/2}\,dw\,, \tag{14.83}$$

which gives the solution $U(x)$ implicitly: typical solutions are illustrated schematically in Fig. 14.16 (b). The boundary conditions $u = 0$ at $x = \pm L/2$ and the

last equation give

$$L = (2D)^{1/2} \int_0^{u_m} [F(u_m) - F(w)]^{-1/2}\,dw \quad \Rightarrow \quad u_m = u_m(L)\,. \tag{14.84}$$

We thus obtain, implicitly, u_m as a function of L. The actual determination of the dependence of u_m on L has to be carried out numerically. Note the singularity in the integrand when $w = u_m$, but because of the square root it is integrable. Typically u_m increases with L as illustrated in Fig. 14.16 (b).

Spatial Patterning of the Spruce Budworm

Now consider the model for the spruce budworm, the dynamics for which we derived in Section 1.2 in Chapter 1. Here, using (1.8) for $f(u)$, (14.77) becomes

$$u_t = ru\left(1 - \frac{u}{q}\right) - \frac{u^2}{1+u^2} + Du_{xx} = f(u) + Du_{xx}\,, \tag{14.85}$$

where the positive parameters r and q relate to the dimensionless quantities associated with the dimensional parameters in the model defined by (1.7); q is proportional to the carrying capacity and r is directly proportional to the linear birth rate and inversely proportional to the intensity of predation. The population dynamics $f(u)$ is sketched in Fig. 14.17 (a) when the parameters are in the parameter domain giving three positive steady states u_1, u_2 and u_3, the first and third being linearly stable and the second unstable. With $F(u)$ defined by (14.82) and substituted into (14.84) we have u_m as a function of the domain size L. This was evaluated numerically by Ludwig et al. (1979) the form of which is shown in Fig. 14.17 (b): there is another critical length, L_0 say, such that for $L > L_0$ more than one solution exists. We analyse this phenomenon below.

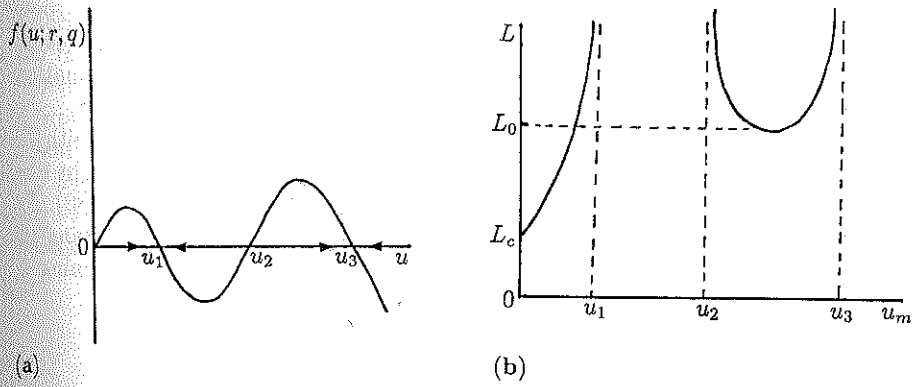

Fig. 14.17a,b. (a) Typical dynamics $f(u;r,q)$ for the spruce budworm as defined by (14.85). (b) The maximum population u_m as a function of the domain size L. For $u_m < u_1$ the population is in the refuge range, whereas $u_m > u_2$ for $L > L_0$, which is in the outbreak regime.

From an ecological viewpoint we would like to know the critical domain size L_0 when the maximum population can be in the outbreak regime; that is $u_m > u_2$ in Fig. 14.17 (a). This is determined from numerical integration of (14.84) and is shown in Fig. 14.17 (b). When $L > L_0$ we see from Fig. 14.17 (b) that there are three possible solutions with different u_m. The ones with u in the refuge and outbreak regimes are stable and the other, the middle one, is unstable. Which solution is obtained depends on the initial conditions. Later we shall consider possible ecological uses of this model in the control of the budworm. Before doing so we describe a useful technique for determining approximate values for L_0 analytically.

Analytical Method for Determining Critical Domain Sizes and Maximum Populations

The numerical evaluation of $u_m(L)$ when there are three possible u_m for a given L is not completely trivial. Since the critical domain size L_0, which sustains an outbreak, is one of the important and useful quantities we require for practical applications, we now derive an *ad hoc* analytical method for obtaining it by exploiting an idea described by Lions (1982).

The steady state problem is defined by (14.81). Let us rescale the problem so that the domain is $x \in (0,1)$ by setting $x \to x/L$ so that the equivalent $U(x)$ is now determined from

$$DU'' + L^2 f(U) = 0, \quad U(0) = U(1) = 0 \,. \tag{14.86}$$

From Fig. 14.16 the solution looks qualitatively like a sine. With the rescaling so that $x \in (0,1)$ the solution is thus qualitatively like $\sin(\pi x)$. This means that $U'' \approx -\pi^2 U$ and so the last equation implies

$$-D\pi^2 U + L^2 f(U) \approx 0 \quad \Rightarrow \quad \frac{D\pi^2 U}{L^2} \approx f(U) \,. \tag{14.87}$$

We are interested in the value of L such that the last equation has three roots for U: this corresponds to the situation in Fig. 14.17 (b) when $L > L_0$. Thus all we need do to determine an approximate L_0 is simply to plot the last equation as in Fig. 14.18 and determine the value L such that three solutions exist.

For a fixed dispersal coefficient D we see how the solutions U vary with L. As L increases from $L \approx 0$ the first critical L, L_c, is given when the straight line $D\pi U/L^2$ intersects $f(U)$; that is when $D\pi^2/L^2 = f'(0)$, as given by (14.80). As L increases further we can determine the critical L_0 when $D\pi^2 U/L_0^2$ is tangent to the curve $f(U)$, at P in the Fig. 14.18. It is just a matter of determining L which gives a double positive root of

$$\frac{D\pi^2 U}{L^2} = f(U) \,.$$

It is left as an exercise (Exercise 7) to determine L_0 as a function of r, q and D when $f(U)$ is given by (14.85). For any given L the procedure also determines,

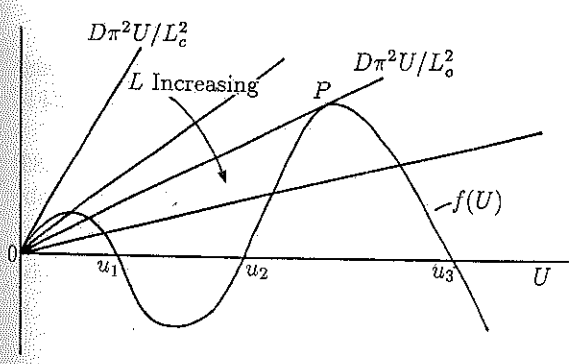

Fig. 14.18. Approximate analytic procedure for determining the critical domain sizes L_c and L_0 which can sustain respectively a refuge and an outbreak in the species population where the dynamics is described by $f(U)$. L_c is the value of L when $D\pi^2 U/L^2$ is tangent to $f(U)$ at $U = 0$. L_0 is given by the value of L when $D\pi U/L^2$ is just tangent to $F(U)$ at P.

approximately, the maximum U. From Fig. 14.18 we clearly obtain by this procedure a similar figure to that in Fig. 14.17 (b). This procedure is quite general for determining critical domain sizes, both for structure bifurcating from the zero steady state and for domains which can sustain larger populations arising from population dynamics with multiple positive steady states.

14.8 Spatial Patterns in Scalar Population Interaction-Reaction Diffusion Equations with Convection: Ecological Control Strategies

In practical applications of such models the domains of interest are usually two-dimensional and so we must consider (14.76). Also, with insect pests in mind, the exterior region is not generally completely hostile, so $u = 0$ on the boundaries is too restrictive a condition. Here we briefly consider a one and two-dimensional problem in which the exterior domain is not completely hostile and there is a prevailing wind. This is common in many insect dispersal situations; it can modify the spatial distribution of the population in a major way.

Suppose, for algebraic simplicity, that the two-dimensional domain is a rectangular region B defined by $0 \le x \le a$, $0 \le y \le b$ having area A. The completely hostile problem is then given by

$$u_t = f(u) + D\left(\frac{\partial^2 u}{\partial x^2} + \frac{\partial^2 u}{\partial y^2}\right) \,, \tag{14.88}$$

$$u = 0 \quad \text{for} \quad (x,y) \text{ on } \partial B \,.$$

Following the same procedure as in the last section for u small we get the solution

of the linearised problem to be

$$u(x,y,t) = \sum_{n,m} a_{mn} \exp\left\{\left[f'(0) - D\pi^2\left(\frac{n^2}{a^2} + \frac{m^2}{b^2}\right)\right]t\right\} \sin\frac{n\pi x}{a} \sin\frac{m\pi y}{b} \tag{14.89}$$

So the critical domain size, which involves both a and b, is given by any combination of a and b such that

$$\frac{a^2b^2}{a^2+b^2} = \frac{D\pi^2}{f'(0)} .$$

Since

$$a^2 + b^2 > 2ab = 2A \quad \Rightarrow \quad \frac{a^2b^2}{a^2+b^2} < \frac{A}{2}$$

we get an inequality estimate for spatial patterning to exist, namely

$$A > \frac{2D\pi^2}{f'(0)} . \tag{14.90}$$

Estimates for general two-dimensional domains have been obtained by Murray and Sperb (1983). Clearly the mathematical problem is that of finding the smallest eigenvalue for the spatial domain considered.

In all the scalar models considered above the spatial patterns obtained have only a single maximum. With completely hostile boundary conditions these are the only type of patterns that can be generated. With two-species reaction diffusion systems, however, we saw that more diverse patterns could be generated. It is natural to ask whether there are ways in which similar multi-peak patterns could be obtained with single species models in a one-dimensional context.

Suppose now that there is a constant prevailing wind $\mathbf{w}$ which contributes a convective flux $(\mathbf{w}\cdot\nabla)u$ to the conservation equation for the population $u(\mathbf{r},t)$. Also suppose that the exterior environment is not completely hostile in which case appropriate boundary conditions are

$$(\mathbf{n}\cdot\nabla)u + hu = 0, \quad \mathbf{r} \text{ on } \partial B , \tag{14.91}$$

where $\mathbf{n}$ is the unit normal to the domain boundary ∂B. The parameter h is a measure of the hostility: $h = \infty$ implies a completely hostile exterior, whereas $h = 0$ implies a closed environment, that is zero flux boundaries. We briefly consider the latter case later. The mathematical problem is thus

$$u_t + (\mathbf{w}\cdot\nabla)u = f(u) + D\nabla^2 u , \tag{14.92}$$

with boundary conditions (14.91) and given initial distribution $u(\mathbf{r},0)$. Here we consider the one-dimensional problem and follow the analysis of Murray and Sperb (1983), who also deal with the two-dimensional analogue and more general aspects of such problems.

The problem we briefly consider is the one-dimensional system which defines the steady state spatially inhomogeneous solutions $U(x)$. From (14.91) and (14.92), since

$$(\mathbf{w}\cdot\nabla)u = w_1 u_x ,$$
$$(\mathbf{n}\cdot\nabla)u + hu = 0 \quad \Rightarrow \quad u_x + hu = 0,\ x = L; \quad u_x - hu = 0,\ x = 0 ,$$

where w_1 is the x-component of the wind $\mathbf{w}$, the mathematical problem for $U(x)$ is

$$\begin{aligned} &DU'' - w_1 U' + f(U) = 0 , \\ &U'(0) - hU(0) = 0, \quad U'(L) + hU(L) = 0 . \end{aligned} \tag{14.93}$$

We study the problem using phase plane analysis by setting

$$U' = V, \quad DV' = w_1 V - f(U) \quad \Rightarrow \quad \frac{dV}{dU} = \frac{w_1 V - f(U)}{DV} , \tag{14.94}$$

and we look for phase plane trajectories which, from the boundary conditions in (14.93), join any point on one of the following lines to any point on the other line:

$$V = hU, \quad V = -hU . \tag{14.95}$$

The phase plane situation is illustrated in Fig. 14.19 (a), (b) as we shall now show.

Refer first to Fig. 14.19 (a). From (14.94) we get the sign of dV/dU at any point (U,V). On the curve $V = f(U)/w_1$, $dV/dU = 0$ with dV/dU positive and negative when (U,V) lies respectively above (if $V > 0$) and below it. So, if we start on the boundary line $V = hU$ at say P the trajectory will qualitatively be like T_1 since $dV/dU < 0$ everywhere on it. If we start at S, say, although the trajectory starts with $dV/dU < 0$ it intersects the $dV/dU = 0$ line and passes through to the region where $dV/dU > 0$ and so the trajectory turns up. The trajectories T_2, T_3 and T_4 are all possible scenarios depending on the parameters and where the solution trajectory starts. T_3 and T_4 are not solution trajectories satisfying (14.94) since they do not terminate on the boundary curve $V = -hU$. T_1 and T_2 are allowable solution paths and each has a single maximum U where the trajectory crosses the $V = 0$ axis.

We now have to relate the corresponding domain length L to these solution trajectories. To be specific let us focus on the trajectory T_2. Denote the part of the solution with $V > 0$ by $V^+(U)$ and that with $V < 0$ by $V^-(U)$. If we now integrate the first equation in (14.94) from U_Q to $U_{Q'}$, that is the U-values at either end of the T_2 trajectory, we get the corresponding length of the domain for the solution represented by T_2 as

$$L = \int_{U_Q}^{U_m} [V^+(U)]^{-1}\, dU + \int_{U_m}^{U_{Q'}} [V^-(U)]^{-1}\, dU . \tag{14.96}$$

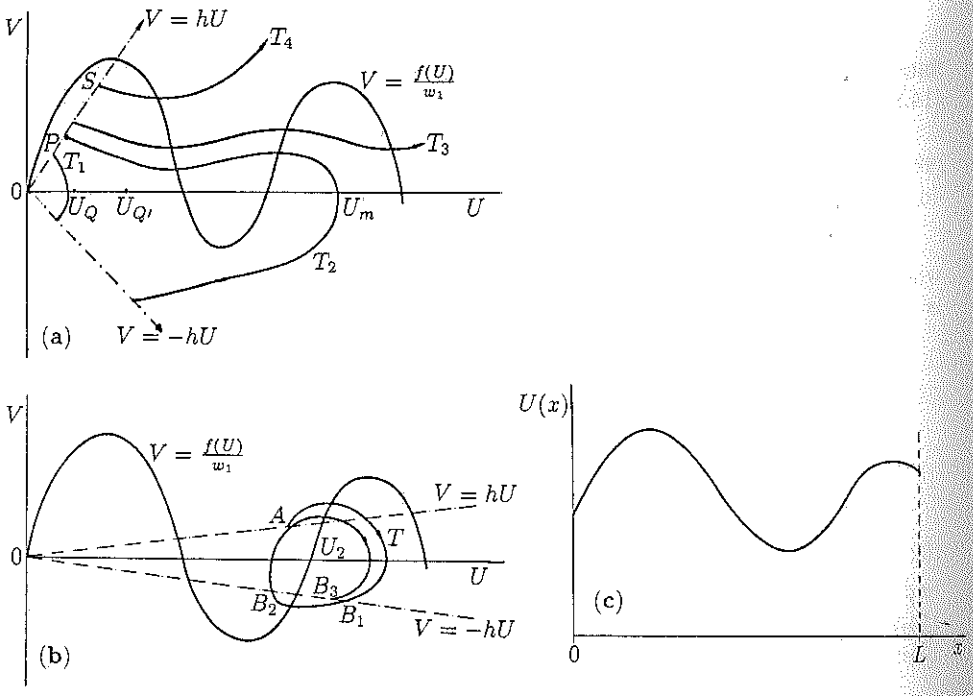

Fig. 14.19a-c. (a) With h sufficiently large the possible trajectories from $V = hU$ to $V = -hU$ admit solution trajectories like T_1 and T_2 with only a single maximum U_m. (b) For small enough h it is possible to have more complex patterns as indicated by the specimen trajectory T. (c) A typical solution $U(x)$ for a phase trajectory like T in (b).

So, for each allowable solution trajectory we can obtain the corresponding size of the solution domain. The qualitative form of the solution $U(x)$ as a function of x can be deduced from the phase trajectory since we know U and U' everywhere on it and from the last equation we can calculate the domain size. With the situation represented by Fig. 14.19 (a) there can only be a single maximum in $U(x)$. Because of the wind convection term, however, there is no longer the solution symmetry of the solutions as in the last Section 14.7.

Now suppose the exterior hostility decreases, that is h in (14.95) decreases, so that the boundary lines are now as illustrated in Fig. 14.19 (b). Proceeding in the same way as for the solution trajectories in Fig. 14.19 (a) we see that it is possible for a solution to exist corresponding to the trajectory T. On sketching the corresponding solution $U(x)$ we see that here there are two maxima in the domain: see Fig. 14.19 (c). In this situation however we are in fact patching several possible solutions together. Referring to Fig. 14.19 (b) we see that a possible solution is represented by that part of the trajectory T from A to B_1. It has a single maximum and a domain length L_1 given by the equivalent of (14.96). So if we restrict the domain size to be L_1 this is the relevant solution. However, if we allow a larger L the continuation from B_1 to B_2 is now possible and so the

trajectory AB_1B_2 corresponds to a solution of (14.93). Increasing L further we can include the rest of the trajectory to B_3. It is thus possible to have multi-humped solutions if the domain is large enough. The length L corresponding to the solution path T is obtained in exactly the same way as above, using the equivalent of (14.96).

So, for small enough values of h it is possible to have more and more structure as the trajectory winds round the point u_2 in the (U, V) phase plane. For such solutions to exist, of course, it is essential that $w_1 \neq 0$. If $w_1 = 0$ the solutions are symmetric about the U-axis and so no spiral solutions are possible. Thus a prevailing wind is essential for complex patterning. It also affects the critical domain size for patterns to exist. General results and further analysis are given by Murray and Sperb (1983).

An Insect Pest Control Strategy

Consider now the problem of insect pest control. The forest budworm problem is very much a two-dimensional spatial problem. As we pointed out in Chapter 1, Section 1.2, a good control strategy would be to maintain the population at a refuge level. As we also showed in Section 1.2 it would be strategically advantageous if the dynamics parameters r and q in (14.85) could be changed so that only a single positive steady state exists. This is not really ecologically feasible. With the more realistic spatial problem, however, we have a further possible means of keeping the pest levels within the refuge range by ensuring that their spatial domains are of a size that do not permit populations in the outbreak regime. The arguments go through for two-dimensional domains, but for illustrative purposes let us consider first the one-dimensional situation.

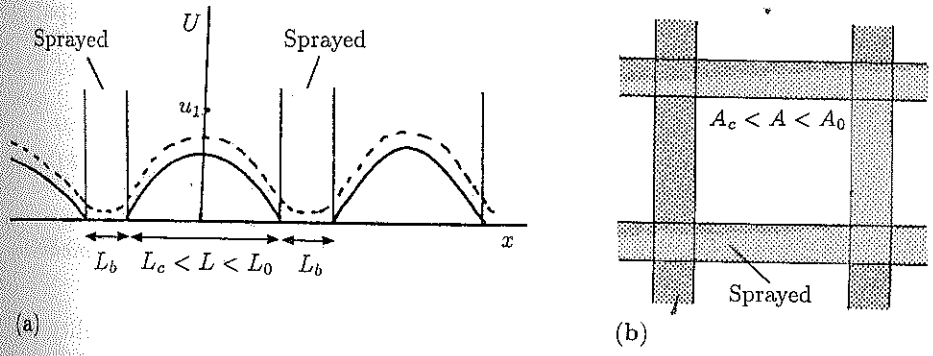

Fig. 14.20a,b. (a) A possible control strategy to contain the insect pest in a refuge rather than an outbreak environment. Strips – insect 'breaks' - are sprayed to maintain an effective domain size $L < L_0$, the critical size for an outbreak. The broken line is more a typical situation in practice. (b) Equivalent two-dimensional analogue where $A > A_c$ is a typical domain which can sustain a pest refuge population but which is not sufficient to sustain an outbreak, that is $A < A_0$.

Refer to Fig. 14.17 (b). If the spatial region was divided up into regions with size $L < L_0$, that is so that the maximum u_m was always less than u_1, the refuge population level, we would have achieved our goal. So, a possible strategy is to spray the region in strips so that the non-sprayed regions impose an effective $L < L_0$ as in Fig. 14.20 (a): the solid vertical lines separating the sprayed regions are the boundaries to a completely hostile exterior.

Of course it is not practical to destroy all pests that stray out of the unsprayed region, so a more realsitic model is that with boundary conditions (14.91) where some insects can survive outside the untreated domain. The key mathematical problem to be solved then is the determination of the critical width of the insect 'break' L_b. This must be such that the contributions from neighbouring untreated areas do not contribute a sufficient number of insects, which diffuse through the break, to initiate an outbreak in the neighbouring patches even though $L < L_0$, the critical size in isolation. A qualitative population distribution would typically be as shown by the dashed line in Fig. 14.20 (a).

The two-dimensional analogue is clear but the solution of the optimisation problem is more complicated. First the critical domain A_0 which can sustain an insect pest outbreak has to be determined for boundary conditions (14.91). Then the width of the sprayed strips have to be determined. It is not a trivial problem to solve, but certainly a possible one. A preliminary investigation of these problems has been carried out by Ben-Yu, Mitchell and Sleeman (1986).

Although we have concentrated on the budworm problem the techniques and control strategies are equally applicable to other insect pests. The field of insect dispersal presents some very important ecological problems, such as the control of killer bees now sweeping up through the western United States (see, for example Taylor (1977)) and locust plagues in Africa. Levin (see for example, 1974, 1976, 1981a,b) has made realistic and practical studies of these and other problems associated with spatially heterogeneous ecological models. The concept of a break control strategy to prevent the spatial spread of a disease epidemic will be discussed in some detail later in Chapter 20 when we discuss the spatial spread of rabies.

*14.9 Nonexistence of Spatial Patterns in Reaction Diffusion Systems: General and Particular Results

Nonexistence of Stable Spatial Patterns for Scalar Equations in One Dimension with Zero Flux Boundary Conditions

Since we found more complex patterns in the last section as the hostility parameter h in (14.91) decreased, it is natural to ask if a single reaction diffusion equation with zero prevailing wind, that is $w = 0$, and zero flux boundary conditions, that is $h = 0$, can sustain *stable* spatial patterns. Here the question of stability is important since zero flux conditions effectively allow for free movement of the population density on the boundaries. So, it is always a possibility

that the solution will just evolve to the uniform steady state. Here we show that *a scalar* reaction diffusion equation cannot sustain a spatial pattern if we restrict it to one space dimension.

Consider the following problem:

$$\begin{aligned} &u_t = f(u) + u_{xx}, \quad x \in (0,1), \quad t > 0 \\ &u_x(0,t) = u_x(1,t) = 0, \quad t > 0\,. \end{aligned} \tag{14.97}$$

Steady state spatially nonuniform solutions $U(x)$ satisfy

$$U'' + f(U) = 0, \quad U'(0) = U'(1) = 0\,. \tag{14.98}$$

We shall prove that if $U(x)$ with $U'(x)$ not identically zero is a solution of (14.98) then $U(x)$ is unstable.

It is sufficient to prove that U is linearly unstable so let

$$\begin{aligned} &u(x,t) = U(x) + w(x,t), \quad |w| \ll |U|_{\max}\,, \\ &w(x,t) = y(x)e^{\lambda t}\,. \end{aligned} \tag{14.99}$$

The solution U is stable if $\mathrm{Re}\,\lambda < 0$. Substitution into (14.97) and retaining only linear terms gives

$$\lambda y = y'' + f'(U(x))y, \quad y'(0) = y'(1) = 0\,. \tag{14.100}$$

We realistically assume that $f'(U)$ is bounded, by $K(>0)$ say. If we consider the eigenvalue problem with K replacing $f'(U)$ we have

$$y'' + (K - \lambda)y = 0, \quad y'(0) = y'(1) = 0$$

which has a discrete set of eigenvalues for $\lambda < K$ and no non-trivial solutions for all $\lambda > K$. This implies that with f' bounded, the discrete eigenvalues λ of (14.100) must be bounded above and so there must be a largest eigenvalue, λ_0 say.

With λ_0 the largest eigenvalue of the set $\lambda_0, \lambda_1, \lambda_2, \ldots$ of the problem defined by (14.100), we have

$$\lambda_0 > \lambda_1 \geq \lambda_2 \ldots$$

Now consider the eigenvalue problem

$$\mu y = y'' + f'(U(x))y, \quad y(0) = y(1) = 0\,, \tag{14.101}$$

that is with fixed boundary values. Note that $z = U'(x)$ is an eigenfunction of (14.101) if $\mu = 0$ since

$$\begin{aligned} &0 = U''' + f'(U)U' \\ &U'(0) = U'(1) = 0 \end{aligned} \quad \Rightarrow \quad \begin{aligned} &z'' + f'(U)z = 0\,, \\ &z(0) = z(1) = 0\,. \end{aligned}$$